Nanoscale Advances

ROYAL SOCIETY OF CHEMISTRY

PAPER

View Article Online
View Journal | View Issue

Cite this: *Nanoscale Adv.*, 2026, **8**, 2003

Multimodal radiosensitization by hafnium oxide nanoparticles and HDAC inhibitors: mechanistic insights

Csenge Bocz,[ab] Dóra Izabella Adamecz,[a] Krisztina Szőke,[a] Bálint Péntek,[a] Emília Rita Szabó,[c] Róbert Polanek,[c] Titanilla Szögi,[d] Andrea Rónavári,[e] Katalin Hideghéty,[cf] Zoltán Kónya,[e] Nóra Igaz †*[ag] and Mónika Kiricsi †*[a]

Radiation therapy is routinely utilized in cancer treatment, often in combination with chemotherapy, but is limited by collateral damage to healthy tissues and radioresistance of some tumors. Radiosensitizing agents can enhance tumor cell susceptibility to ionizing radiation, allowing effective treatment at lower doses. High-atomic-number metal-based nanoparticles, such as hafnium oxide (HfO_2NP), can locally amplify the impact of ionizing radiation on cancer cells, augment the radiation-triggered generation of reactive electrons and oxygen species (ROS), induce DNA damage, and ultimately lead to cell death. We hypothesized that this effect can be further enhanced by histone deacetylase (HDAC) inhibitors, which maintain the chromatin in a relaxed state and render the DNA more accessible to genotoxic stress. In this study, we found that HfO_2NPs and the HDAC inhibitor, when combined with irradiation, induced significantly higher ROS production, massively reduced mitochondrial membrane potential, and increased DNA double-strand break formation in cancer cells compared to untreated or single-agent-treated cells. These effects led to a marked reduction in colony-forming potential in both 2D and 3D models and induced significant apoptosis. No cytotoxicity was observed in non-cancerous fibroblasts. HfO_2NPs and the tested HDAC inhibitor form a remarkably efficient cancer-selective radiosensitizing combination, where the enzyme inhibitor facilitates the irradiation-induced DNA-damaging potential of the nanoparticles. This outstanding multimodal approach can target radioresistant cancer cells, while not affecting healthy cells, underscoring its potential in a next-generation nanomedicine-based radiosensitizing strategy to attenuate cancer cell growth for an improved therapeutic outcome.

Received 2nd September 2025
Accepted 12th February 2026

DOI: 10.1039/d5na00845j

rsc.li/nanoscale-advances

Introduction

In addition to conventional chemotherapy, radiation therapy is a commonly used anti-cancer modality that employs ionizing radiation to reduce the size and the metastatic potential of solid tumors and enhance the efficiency of chemotherapy. Ionizing radiation exerts its effects both directly by damaging the membrane structures and DNA, and indirectly, *via* the generation of reactive oxygen species that induce injury to macromolecules, cellular components, and organelles. However, as ionizing radiation is not specific to tumors, radiation therapy can provoke undesired side effects due to its impact on healthy tissues surrounding the tumor. It also carries a secondary risk of potential carcinogenic effects, in particular when high-dose radiation is applied. Therefore, to improve the efficiency of radiotherapy and prevent or minimize the harm to normal cells, radiosensitizers can be utilized to selectively augment tumor sensitivity to radiation.[1–3]

Metal-based nanoparticles have become increasingly prominent in medicine owing to their distinctive and remarkably unique physical, chemical, and optical characteristics. One of their most compelling advantages lies in their ability to passively and preferentially accumulate in tumor tissues, a phenomenon facilitated by the enhanced permeability and retention effect. Additionally, their large specific surface enables extensive and easy functionalization with targeting ligands or coating materials to further enhance cancer selectivity while simultaneously avoiding their recognition and clearance by the immune system. This combination of passive

[a]*Department of Biochemistry and Molecular Biology, University of Szeged, Szeged, Hungary. E-mail: kiricsim@bio.u-szeged.hu; kiricsim@gmail.com*

[b]*National Academy of Scientist Education, National Biomedical Foundation, Szeged, Hungary*

[c]*ELI-ALPS, ELI-HU Non-Profit Ltd, Szeged, Hungary*

[d]*Department of Pathology, University of Szeged, Szeged, Hungary*

[e]*Department of Applied and Environmental Chemistry, University of Szeged, Szeged, Hungary*

[f]*Department of Oncotherapy, University of Szeged, Szeged, Hungary*

[g]*Incubation Competence Centre of the Centre of Excellence for Interdisciplinary Research, Development and Innovation of the University of Szeged (SZTE IKIKK), Szeged, Hungary. E-mail: nora.igaz@bio.u-szeged.hu*

† These authors contributed equally to this work.

and active targeting highlights their growing potential in oncotherapy.[4,5] Metal-based nanoparticles composed of high-atomic-number (high-Z) elements are recognized as promising radiosensitizing agents, capable of significantly amplifying the damaging effect of ionizing radiation *via* physical, chemical, and biological enhancement mechanisms. In the physical phase of dose enhancement, the interaction between ionizing radiation and high-Z metal-based nanoparticles induces a photoelectric effect followed by the Auger cascade and Compton effect. These interactions result in the ejection of a cascade of low-energy secondary electrons, both from the inner and outer electron shells. This in turn amplifies the localized energy deposition and intensifies radiation-induced damage at the cellular level. Subsequently, the emitted secondary electrons along with the primary ionizing radiation interact with water molecules, leading to the generation of reactive oxygen species (ROS), which ultimately impose extensive oxidative stress on vital cellular macromolecules, including DNA, membrane lipids, structural proteins, enzymes, and harm cellular organelles. The accumulation of uncorrected damages disrupts essential cellular functions, overwhelms repair mechanisms, causes cell cycle arrest, culminating in apoptotic, necrotic, or other types of cell death.[6–8]

Hafnium oxide nanoparticles (HfO_2NPs) have emerged as outstanding candidates for the purpose of the above-detailed radiosensitization owing to the intrinsically favorable physicochemical properties of hafnium. As a chemically stable metal with a high atomic number ($Z = 72$) and electron density, hafnium is particularly well-suited for enhancing the local deposition of radiation energy. Among high-Z inorganic nanomaterials, HfO_2NPs distinguish themselves by their favorable biocompatibility, low toxicity, and robust safety profile. Beyond the promising radiosensitizing capabilities, HfO_2NPs offer valuable multifunctional utility as X-ray and computed tomography (CT) imaging contrast agents or as nanocarrier systems suitable for drug-delivery of chemotherapeutic compounds. Their surface modifiability, combined with excellent *in vitro* and *in vivo* biocompatibility, enables versatile biomedical applications.[9,10] The clinical relevance of hafnium-based nanomaterials is underscored by the development of NBTXR3, a 50 nm-sized, spherical, phosphate-functionalized HfO_2NPs formulation, which is currently undergoing clinical phase I and II trials. Furthermore, ongoing research is exploring the impact of HfO_2NPs on many types of solid tumors, including soft tissue sarcomas, head and neck cancers, and pancreatic malignancies.[11–15] Recent studies have highlighted the immunomodulatory properties of HfO_2NPs. Specifically, treatment with hafnium-based nanoparticles has been shown to potentiate anti-tumor immune responses *via* activation of the cyclic GMP-AMP synthase (cGAS) – stimulator of interferon genes (STING) pathway. This dual functionality, combining localized radiotherapeutic enhancement with systemic immune activation, suggests another level of synergistic mechanism that may broaden the therapeutic impact of hafnium-based nanoparticles.

A growing number of clinically approved chemotherapeutic agents are already recognized for their radiosensitizing properties. Among these, histone deacetylase (HDAC) inhibitors – used in the treatment of different types of hematologic malignancies and solid tumors – stand out as they have demonstrated a particularly notable capacity to potentiate the ionizing radiation-induced cytotoxicity. In numerous cancer types, protein homeostasis becomes dysregulated, a vulnerability that can be therapeutically exploited by HDAC inhibition. HDAC enzymes regulate the acetylation of histone and non-histone proteins, influencing protein stability, protein–protein interactions, binding affinities, and subcellular localization of proteins.[16,17] By modulating the acetylation patterns of certain proteins, HDAC inhibitors can interfere with key oncogenic pathways, impair tumor progression, suppress cancer cell invasion and metastasis, and sensitize cancer cells to other anticancer modalities, including radiation. Mechanistically, histone deacetylase inhibition has been shown to induce both apoptosis and autophagy in cancer cells, independent of p53 status, *via* the modulation of multiple pro-apoptotic and anti-apoptotic mediators, such as p21 protein, stress-activated protein kinase (SAPK), B-cell lymphoma 2 (Bcl-2), B-cell lymphoma extra-large (Bcl-xL), Bax, or tumor necrosis factor-related apoptosis-inducing ligand (TRAIL) proteins.[18–27] Importantly, HDAC inhibitors can sensitize tumor cells to irradiation by disrupting DNA repair pathways. In particular, they downregulate critical components of the homologous recombination and non-homologous end-joining mechanisms, including Rad51, BRCA2, Rad50, MRE11, Ku70, Ku80, and DNA-PKcs, thereby impairing the cell's capacity to recover from radiation-induced DNA damage.[28–30] Moreover, the inhibition of HDAC enzymes results in the hyperacetylation of histone proteins at the N-terminal lysine residues, leading to chromatin decondensation. The relaxed chromatin structure enhances DNA accessibility and renders it vulnerable and more susceptible to genotoxic effects, such as ionizing radiation or ROS. Collectively, these multifactorial mechanisms support the strategic utilization of HDAC inhibitors not only as standalone chemotherapeutics but also as effective radiosensitizers within combinational treatment regimens.[31,32]

In two of our previous studies, we demonstrated that HDAC inhibitors can act as effective chemo- and radiosensitizers when used in pharmacological co-administration with noble metal-based nanoparticles. We showed that the HDAC inhibitor trichostatin A (TSA) enhances the cytotoxic effect of silver nanoparticles (AgNPs), while SAHA, another HDAC inhibitor, synergizes with gold nanoparticles (AuNPs) under ionizing radiation, resulting in a marked amplification of their radiosensitizing effects. These findings led us to propose that HDAC inhibitors may facilitate chromatin relaxation, thereby rendering the DNA more accessible to harmful agents, including silver ions and reactive electrons deriving from noble metal-based nanoparticles, as well as ionizing radiation, ultimately triggering DNA damage and promoting cancer cell death. Given the compelling therapeutic synergy observed with both of the HDAC inhibitor – noble metal-based nanoparticle combinations, a critical issue arose. Is this valuable enhancement of biological efficacy by HDAC inhibitors restricted to noble metals, or can it be generalized to other high-Z metal or

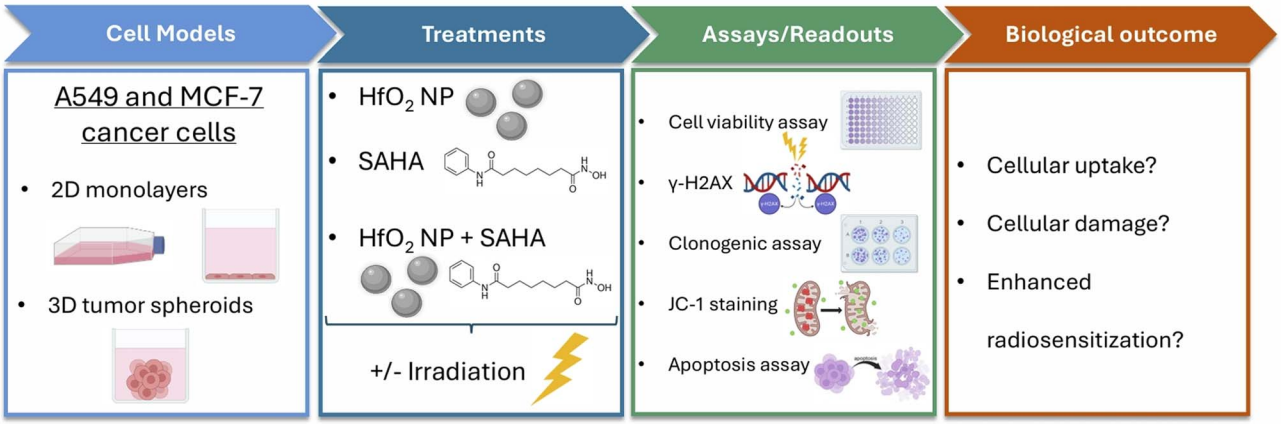

Fig. 1 Schematic workflow describing the cell models, the treatment types, the utilized assays, and the possible biological outcomes.

metal oxide nanoparticles, such as HfO_2NPs as well? This question is particularly relevant as HfO_2NPs are already undergoing clinical evaluations, and elucidating their interaction with HDAC inhibitors may pave the way for a new class of combinational cancer therapeutic approaches. Therefore, the present study was undertaken to investigate whether the pharmacological co-administration of SAHA and hafnium oxide nanoparticles could enhance the response of cancer cells to ionizing radiation (Fig. 1). Recognizing the limitations of conventional 2D cultures in mimicking the tumor microenvironment, we expanded our investigation to include 3D spheroid models, which much better recapitulate the structural complexity, the drug penetration barriers, and radiation response of solid tumors (Fig. 1). By exploring this combination across multiple cancer cell lines, we aimed to uncover both the mechanistic basis and translational relevance of this novel therapeutic strategy.

Materials and methods

2D and 3D cell cultures

MCF-7 human breast adenocarcinoma and A549 human lung adenocarcinoma cell lines were employed in the study, as MCF-7 cells are known for their radiosensitivity, while A549 cells exhibit radioresistance. Moreover, to test the tumor-specific effects of the treatments, non-cancerous MRC-5 fibroblasts were used. MCF-7 cells (ATCC) were cultured in RPMI medium (Biosera, Cholet, France) supplemented with 10% fetal bovine serum (FBS, Biosera, Cholet, France), 2 mM glutamine (Biosera, Cholet, France), 0.01% streptomycin, and 0.005% penicillin (Biosera, Cholet, France). A549 cells were maintained in Dulbecco's Modified Eagle Medium (DMEM, Biosera, Cholet, France) containing 1 g L^{-1} glucose, 10% FBS (Biosera, Cholet, France), 2 mM glutamine (Biosera, Cholet, France), 0.01% streptomycin, and 0.005% penicillin (Biosera, Cholet, France). MRC-5 cells were maintained in MEM medium (Biosera, Cholet, France) complemented with 10% FBS (Biosera, Cholet, France), 2 mM glutamine (Biosera, Cholet, France), 0.01% streptomycin, and 0.005% penicillin (Biosera, Cholet, France). All the cell types were maintained under standard conditions at 37 °C, with 5% CO_2 and 95% humidity.

To create 3D cell cultures, 10 000 cells/well were seeded into ultra-low attachment U-bottom 96-well microtiter plates (Thermo Fisher Scientific, Waltham, Massachusetts, USA). The plates were then centrifuged at a speed of 1000 rpm for 5 minutes, allowing the cells to settle and aggregate at the bottom of each well. Following this step, the plates were incubated at 37 °C with 5% CO_2 and 95% humidity for a duration of one week to form the spheroids.

Hafnium oxide nanoparticles

HfO_2 nanoparticles were purchased from Nanografi as a 99.99% pure powder. The average size of the nearly spherical-shaped nanoparticles ranged from 55 to 75 nm. To suspend the nanoparticles in distilled water, citrate was added in a 10 : 1 mass (w/w) ratio to ensure stability. A stock solution with a concentration of 1200 μg mL^{-1} was prepared, which was then homogenized by sonication (LBS1 Ultrasonic bath, Falc Instruments, Treviglio, Italy) for 15 minutes before each treatment.

Characterization of the nanoparticles

The purchased nanoparticles were subjected to physicochemical characterization to validate their size distribution, morphology, and surface charge using transmission electron microscopy (TEM), dynamic light scattering (DLS), and zeta potential measurements. TEM images were assessed by a FEI Tecnai G2 20 X-Twin (Hillsboro, OR, USA) transmission electron microscope at an acceleration voltage of 200 kV. The hydrodynamic size and surface charge measurements were performed using a Zetasizer Nano ZS instrument (Malvern, Worcestershire, UK).

Transmission electron microscopy

To visualize the uptake of HfO_2NPs by cancer cells, TEM analysis was performed. For this, 10^5 cells were seeded onto 0.4 μm pore size polyester membrane inserts placed in a 24-well plate (Thermo Fisher Scientific, Waltham, Massachusetts, USA). On

the following day, the cells were treated with 60 μg mL^{-1} of HfO_2NPs for 24 hours. Then, cells were washed with PBS and fixed in 4% glutaraldehyde. Samples were embedded in gelatin and then sliced into 1–2 mm cubes, which were subsequently embedded in epoxy (Embed 812, EMS, PA 19440). To identify the cell monolayer, first semi-thin sections of 1 μm were prepared, then thin sections of 70 nm were obtained and stained with uranyl and lead solutions. Images were captured by a Jeol JEM-1400 electron microscope (Jeol Ltd, Tokyo, Japan) using 100 kV voltage.

Irradiation

The cells were irradiated at the ELI-ALPS Laser Research Institute. Irradiation was performed with 250 keV photons produced by a cell and small animal irradiator (RS320, Xstrahl Limited, Xstrahl Surrey, UK). The samples were irradiated with 0, 2, and 4 Gy at a dose of 3.65 Gy min^{-1}. In all cases, the samples were placed in a special polymethyl methacrylate plate phantom in order to ensure the homogeneity of the irradiation. The isocenter was located in the geometric center of the sample holders.[33] The administered doses were checked with dosimetric measurements using film dosimetry (Gafchromic EBT3). Non-irradiated (0 Gy) cells were also transported to the irradiation site to ensure that the stress experienced during transit would not lead to differences between the samples.

HfO_2NP and SAHA treatments

Cells were divided into four experimental groups based on nanoparticle and HDAC inhibitor treatments: (1) untreated control group, (2) cells treated with SAHA alone at a concentration of 0.3 μM, (3) cells receiving HfO_2NPs at a concentration of 60 μg mL^{-1}, (4) cells receiving both SAHA (0.3 μM) and HfO_2NPs (60 μg mL^{-1}) to assess their combined effects. Nanoparticles and SAHA were applied as a physical co-treatment, not as a chemically or physically conjugated nanoformulation. Treatments were applied typically 24 hours after seeding cells into the plates. Following a 24-hour incubation with the indicated agents, cells were exposed to ionizing radiation at doses of 0, 2, or 4 Gy, where 0 Gy means no irradiation was exerted on the particular samples. This design resulted in a total of 8 or 12 experimental conditions per cell type, depending on whether two or three different radiation doses were employed. Minor variations in sample number occurred in a few isolated cases.

MTT cell viability assays

The impact of HfO_2 nanoparticles on cell viability (without the presence of SAHA or irradiation) was assessed using the MTT assay. For this, A549 and MCF-7 cells were seeded (10 000 cells/well) in 96-well plates, and the next day were treated with varying concentrations (7.5 μg mL^{-1}, 15 μg mL^{-1}, 30 μg mL^{-1}, 60 μg mL^{-1}, and 120 μg mL^{-1}) of HfO_2NPs.

To test the effect of SAHA, HfO_2NPs, and the combination of HfO_2NPs and SAHA on the viability of A549 and MCF-7 cells, as well as non-cancerous MRC-5 fibroblasts, 10 000 cells were seeded into a 96-well plate. On the following day, cells were treated with either 0.3 μM SAHA, 60 μg mL^{-1} HfO_2NPs, or the combination of them for 24 hours. In order to evaluate the impact of ionizing radiation on these cells, the samples were irradiated with 0, 2, or 4 Gy doses on the next day.

When cells received the appropriate treatment/s for 24 hours, the solutions were removed, and the cells were thoroughly washed with PBS. Next, the proper culture medium containing 0.5 mg mL^{-1} MTT reagent (Thermo Fisher Scientific, Waltham, Massachusetts, USA) was added to the samples, and the cells were incubated with it for an hour. The resulting formazan crystals were then dissolved in dimethyl sulfoxide (DMSO, Molar Chemicals Kft, Halásztelek, Hungary), and the absorbance of the samples was assessed using a Synergy HTX plate reader (BioTek, Biotek Instruments lnc, Winooski, VT, USA) set at 570 nm.

Lactate dehydrogenase-based cytotoxicity assay

The cytotoxic effect of SAHA, HfO_2NPs, and their combination was tested on MRC-5 non-cancerous fibroblast cells by lactate dehydrogenase (LDH) assay using Cayman LDH Cytotoxicity Assay Kit (Cayman Chemicals, Ann Arbor, Michigan, USA). For this, 10 000 MRC-5 cells/well were seeded into 96-well plates. On the following day, the cells were treated with 0.3 μM of SAHA, 60 μg mL^{-1} HfO_2NPs, or with their combination for 24 hours, then the samples were irradiated with 0 or 4 Gy doses on the next day. After a 24-hour incubation, 100 μL of supernatant was transferred to a new 96-well plate and incubated for 30 minutes with the LDH reaction solution prepared according to the instructions of the manufacturer. The absorbance of the samples was measured with the Synergy HTX plate reader (BioTek, BioTek Instruments lnc, Winooski, VT, USA) at 490 nm.

Immunocytochemistry

To validate the action of the HDAC inhibitor SAHA on cancer cells, the level of acetylated lysines (ac-Lys) coupled with tubulin immunostaining was determined by immunocytochemistry. Immunocytochemistry was also applied to visualize the DNA double-strand breaks induced by the treatments. For this, γ-H2AX-specific signals were detected. In both cases, the cells were plated at a density of 1×10^5 into 24-well plates (VWR, Radnor, Pennsylvania, USA) on glass coverslips (VWR, Radnor, Pennsylvania, USA). Treatments with SAHA, HfO_2NPs, and their combination were administered on the following day, and each treatment lasted for 24 hours. In the case of ac-Lys immunostaining, the samples were then fixed in 4% formaldehyde (Molar Chemicals Kft, Halásztelek, Hungary). For γ-H2AX immunocytochemistry, after incubation with SAHA, HfO_2NPs, or their combination, the cells were also irradiated, and after 1 hour of incubation, the cells were fixed in 4% formaldehyde (Molar Chemicals Kft, Halásztelek, Hungary).

For the actual immunostaining, the samples were first washed with PBS and incubated with 0.3% Triton-X-100 solution (Molar Chemicals, Halásztelek, Hungary) for 20 minutes. After another wash with PBS, blocking was performed using 5% bovine serum albumin (BSA, Sigma-Aldrich, St Louis, Missouri, USA) solution for 20 minutes, followed by additional washing with PBS. The primary antibodies anti-ac-Lys (Abcam,

Cambridge, UK) and anti-phospho-γ-H2AX (Ser139, Invitrogen, Waltham, Massachusetts, USA) were diluted 1 : 300 in 1% BSA solution. After 1.5 h incubation at room temperature with the primary antibody, the samples were washed twice with PBS. The Alexa-568 or Alexa-488-conjugated (Abcam, Cambridge, UK) secondary antibodies were prepared in 1 : 600 dilutions in 1% BSA solution and were applied onto the samples for 90 minutes. After this, samples were washed twice with PBS, and the cells aimed for γ-H2AX visualization were stained with 1 μg mL^{-1} DAPI (Enzo Life Sciences, Farmingdale, New York, USA) diluted in PBS for 15 minutes before being washed twice with PBS. In the case of ac-Lys-stained samples, images were taken using an Olympus BX51 microscope with an Olympus DP70 camera (Olympus, Tokyo, Japan), while the γ-H2AX-stained samples were examined using an Olympus FV10i confocal microscope (Olympus, Tokyo, Japan). For enhanced visualization, the images taken from the γ-H2AX-stained samples were digitally recolored, with Alexa-488 appearing blue and DAPI appearing red.

Clonogenic assay

To determine the colony-forming capability of the treated cells, clonogenic assays were performed. For this, cells were seeded in 6-well plates (VWR, Radnor, Pennsylvania, USA) at a density of 700 cells/well and immediately treated with 0.3 μM SAHA, 60 μg mL^{-1} HfO_2NPs, or a combination of both agents. After 24 hours, the samples were subjected to irradiation at doses of 0, 2, or 4 Gy and then incubated for one week. After this incubation period, the colonies were fixed using a solution of 70% ethanol and 30% acetone, followed by staining with a 0.5% crystal violet in a 25% methanol solution. Finally, the number of colonies was counted.

3D tumor cultures were subjected to treatment with 90 μg mL^{-1} HfO_2NPs, 0.9 μM SAHA, or their combination, and irradiated similarly to 2D cultures using 0, 2, and 4 Gy doses. After a 24-hour incubation period, the treatments were removed, and 100 μL of Accumax was added to each sample. Following a 10-minute incubation, a single cell suspension was obtained from the spheroids, and the appropriate volumes were transferred to 6-well plates to achieve a concentration of 700 cells. These cell suspensions were incubated for a week to allow the formation of colonies, which were then fixed, stained, and counted identically as in the case of the 2D cultures.

DCFDA staining

DCFDA staining was performed to detect the reactive oxygen species generated intracellularly upon individual SAHA, HfO_2NP, and HfO_2NP + SAHA combination treatments. For this, 1×10^5 cells/well were seeded onto glass coverslips (VWR, Radnor, Pennsylvania, USA) placed in a 24-well plate (VWR, Radnor, Pennsylvania, USA). The following day, the cells were treated with 0.3 μM SAHA, 60 μg mL^{-1} HfO_2NP, or their combination for 24 hours. After the incubation, the samples were irradiated with 0 or 2 Gy radiation doses and incubated for an additional 1 hour. Then the cells were washed in PBS and incubated with 10 μM DCFDA solution diluted in PBS for 20 minutes at 37 °C. The fluorescent intensity of the cells was visualized by an Olympus BX51 microscope equipped with an Olympus DP70 camera (Olympus, Tokyo, Japan) and was quantified using ImageJ software.

JC-1 staining

To investigate the mitochondrial-damaging effects of the treatments, JC-1 staining was conducted. Tumor cells were cultured in 24-well plates, on glass coverslips (VWR, Radnor, Pennsylvania, USA). The following day, the cells were treated with either 0.3 μM SAHA, 60 μg mL^{-1} HfO_2NP, or a combination of both, followed by irradiation after 24 hours. JC-1 dye was then added to the samples at a concentration of 10 μg mL^{-1} diluted in complete culture medium. Cells were incubated with the dye for 15 minutes at 37 °C, then washed twice with PBS. The samples were examined using an Olympus BX51 microscope, images were captured with an Olympus DP70 camera (Olympus, Tokyo, Japan), and the intensity of the red/green fluorescent signal was quantified using ImageJ software.

RNA isolation and quantitative PCR

The endoplasmic reticulum (ER) stress and unfolded protein response (UPR) inducing effect of HfO_2NPs and SAHA was examined by quantitative PCR (qPCR) technique. For these experiments, 6×10^5 cells were seeded into T25 cell culture flasks and treated with 0.3 μM SAHA, 60 μg mL^{-1} HfO_2NPs, or a combination of both for 24 hours. Following this treatment, the cultures were irradiated with doses of 0, 2, or 4 Gy. After 3 hours upon irradiation, the samples were lysed and stored in RLT buffer with 1% β-mercaptoethanol at −80 °C for future examination. Total RNA was isolated according to the Qiagen RNeasy Mini Kit protocol, adhering to the manufacturer's recommendations (Qiagen, Hilden, Germany). Reverse transcription was carried out using the TaqMan Reverse Transcription Kit (Thermo Fisher Scientific, Waltham, Massachusetts, USA), converting 2 μg of RNA into cDNA in a final volume of 50 μL.

The expression levels of the following eight ER stress and UPR markers were assessed using qPCR: binding immunoglobulin protein (BiP), C/EBP homologous protein (CHOP), activating transcription factor 4 (ATF4), ER degradation-enhancing alpha-mannosidase-like protein (EDEM), activating transcription factor 6 (ATF6), heat shock protein 90 kDa beta member 1 (GRP94, also known as endoplasmin), and X-box binding protein 1 (XBP1), including both segmented (XBP1s) and total forms (XBP1t). We utilized primers at a concentration of 200 nM, while the reference gene glyceraldehyde-3-phosphate dehydrogenase (GAPDH) was used at a concentration of 100 nM. SI Table S1 shows the sequences of the primers. The PCR reactions were conducted using the PikoReal Real-time PCR system (Thermo Fisher Scientific, Waltham, Massachusetts, USA) with SYBR Green qPCR Master Mix (Thermo Fisher Scientific, Waltham, Massachusetts, USA), in a total volume of 8 μL, which included 1 μL of cDNA template.

Apoptosis detection

To investigate whether apoptosis occurs upon the treatments, the Apo-ONE Homogeneous Caspase-3/7 assay was performed. For this, 2000 cells/well were seeded into a 96-well plate and left to grow. The next day, the cells were treated with 0.3 μM SAHA, 60 μg mL^{-1} HfO_2NPs, or their combination for 24 hours. Then the cells were irradiated with a 2 Gy dose and incubated for an additional 5 days. Then Apo-ONE Caspase-3/7 Reagent, prepared according to the manufacturer's instructions, was added to the samples in a 1 : 1 ratio. After 3 hours of incubation, the fluorescence of the samples was measured at an excitation wavelength of 485/20 nm and an emission wavelength of 528/20 nm by Synergy HTX Plate reader (BioTek, Biotek Instruments lnc, Winooski, VT, USA).

Statistics

Statistical evaluation of the results was performed using GraphPad Prism 6 software, using one-way ANOVA, Dunnett's multiple comparisons tests (MTT assay, Apo-ONE assay, QPCR results), one-way ANOVA, Tukey's multiple comparisons tests (DCFDA staining, γ-H2AX staining, Ac-Lys immunocytochemistry, JC-1 staining), two-way ANOVA, Tukey's multiple comparisons test (Clonogenic assay), and two-way ANOVA, Sidak's multiple comparisons test (MTT assay, LDH assay, and Clonogenic assay on MRC-5 cells).

Results

Characterization of HfO_2NPs, their uptake by tumor cells, and effect on cell viability

TEM images verified the approximate size and the quasi-spherical morphology of the HfO_2NPs (Fig. S1A). Based on the DLS, the average hydrodynamic diameter of the nanoparticles was approximately 90.75 nm (Fig. S1B). The zeta potential of the nanoparticles was -62.3 ± 10 mV, indicating a highly negative surface charge that provides stability for the colloid solution.

After verifying the size, morphology, and surface charge of the nanoparticles, we next aimed to assess whether HfO_2 nanoparticles influence cellular viability and whether they are efficiently taken up by tumor cells. To this end, MTT assays were performed in which cells were exposed to increasing concentrations of HfO_2 nanoparticles for 24 hours. The cell viability of A549 and MCF-7 cells remained largely unchanged until 15 μg mL^{-1} nanoparticle concentrations (Fig. S2). In the case of A549 cells, a small but statistically significant reduction in viability was observed at 30 μg mL^{-1}, and for MCF-7 cells at 60 μg mL^{-1}. Although we found that the number of living cells continuously decreased with the increasing HfO_2NPs concentration in both cell lines, nevertheless, the observed toxic effects exerted by these nanoparticles can be generally considered as minor at least in the applied concentration range. Based on these results, the concentration of 60 μg mL^{-1} HfO_2NP was selected to be applied on cells in the subsequent experiments. We have to emphasize here that our goal was not to kill cells directly with the nanoparticles, but to find a suitably low nanoparticle concentration where, together with the HDAC inhibitor and/or irradiation, the sensitizing feature of the nanoparticles can be observed and properly examined on both sensitive and radioresistant cancer cells.

Next, we aimed to verify that cancer cells can efficiently take up HfO_2NPs and, as a consequence, high amounts of nanoparticles accumulate within cells. TEM image analysis was performed, which indicated massive cellular internalization of the nanoparticles. Significant accumulation of HfO_2NPs was verified in the cytoplasm of both A549 and MCF-7 cells, albeit no particles were found in the nucleus or in the mitochondria of these cancer cells (Fig. 2).

The HDAC inhibitor SAHA significantly potentiates the ionizing radiation-induced cytotoxicity of HfO_2NP, and their combination reduces the colony-forming capacity of cancer cells

After the uptake and the rather weak cytotoxicity of the HfO_2NPs were verified in both tumor cell cultures, we wanted to examine how the combination of these nanoparticles with the HDAC inhibitor SAHA, without and with ionizing radiation, impacts these cancerous cells. The proper concentration of SAHA (0.3 μM) was selected based on the results of a previous project involving the A549 and MCF-7 cell lines.[32]

The viability of both cell types was examined by MTT assays, where cells were divided into 4 groups: untreated control group, cells treated only with SAHA, cells exposed only to HfO_2NPs, and cells receiving both SAHA and HfO_2NPs in a pharmacological co-administration, to assess their combined effects. Without any irradiation (0 Gy columns in both panels), no noticeable cytotoxicity was observed in any of the samples following individual SAHA, HfO_2NP, or combined treatments, both in A549 and in MCF-7 cells, although nanoparticle-exposed cells exhibited slightly lower viability as a tendency (Fig. 3).

To evaluate the potential of SAHA with hafnium oxide nanoparticles as an effective chemo- and radiosensitizer combination, A549 and MCF-7 cells were subjected to irradiation of 2 and 4 Gy doses following the chemotherapeutic pretreatments described above, and again MTT viability assays were performed. These experiments showed that in A549 cells, treatments of HfO_2NPs alone or in combination with SAHA reduced somewhat the cell viability at 2 and 4 Gy doses, however, the loss of viable cells was statistically significant only

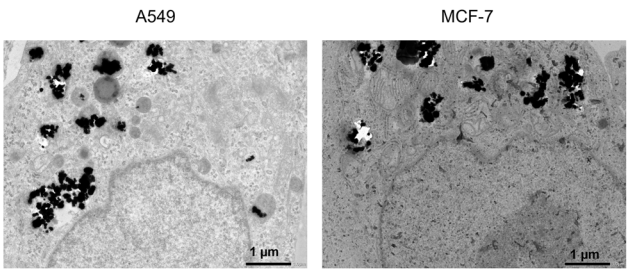

Fig. 2 Internalization of hafnium oxide nanoparticles within cancer cells. Representative TEM images of HfO_2NP-treated A549 and MCF-7 cells indicate internalization of large amounts of HfO_2NPs in the cytoplasm of both cancerous cell types. Scale bar: 1 μm.

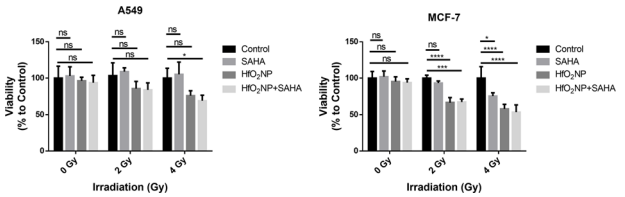

Fig. 3 Viability of A549 and MCF-7 cells treated with SAHA (0.3 μM), HfO_2NPs (60 μg mL^{-1}), and their combination upon no irradiation (0 Gy), and after irradiation with 2 Gy as well as 4 Gy doses. Two-way ANOVA, Tukey's multiple comparisons test, ****P < 0.0001, ***P < 0.001, *P < 0.05.

for SAHA + HfO_2NP and 4 Gy irradiation (Fig. 3). As expected, MCF-7 cells were more sensitive to the treatments than A549 cells, as both HfO_2NPs alone or in combination with SAHA significantly diminished the viability of MCF-7 cells both at 2 Gy as well as at 4 Gy dose radiation treatment. We have to note that a significant decrease in viability was also observed by SAHA exposure when MCF-7 cells were subjected to a 4 Gy irradiation dose (Fig. 3). These results indicated that HfO_2NPs individually and/or in combination with the HDAC inhibitor SAHA can enhance the cancer cell-damaging toxic effect of ionizing radiation, especially when applied in 2 Gy or rather in 4 Gy doses.

In order to check whether the HDAC inhibitory activity of SAHA is not lost if this agent is applied at this concentration together with the nanoparticles, we performed immunostaining on both cell lines to detect the level of acetylated Lys residues, since the aftermath of SAHA action is an increased quantity of acetylated proteins. A549 and MCF-7 cells were exposed to SAHA, administered alone as well as in combination with HfO_2NPs, and the level of acetylated lysines was determined by fluorescence microscopy (Fig. S3). The acetylation level upon SAHA and HfO_2NP + SAHA combinational treatments was significantly higher than the fluorescence intensity of the untreated control or of the cells exposed only to HfO_2NPs (Fig. S3). This analysis clearly verifies that SAHA is able to maintain its HDAC-inhibiting role when it is applied in a pharmacological co-administration with HfO_2NPs.

In the next experiment, we investigated the combined effects of SAHA, HfO_2NPs, and ionizing radiation on the proliferation and colony-forming ability of tumor cells (Fig. 4). The clonogenic assay serves as a gold standard method for assessing the long-term proliferative capacity of tumor cells exposed to ionizing radiation or cytotoxic agents. By quantifying the ability of a single cell to survive treatment and form a colony, this assay provides a robust measure of reproductive cell death and enables the evaluation of the sustained impact of the therapeutic intervention on cellular viability and colony formation potential of tumor cells.

In the absence of ionizing radiation (0 Gy), neither HfO_2 nanoparticles nor SAHA, alone or in combination, affected the colony-forming capacity of A549 cells (Fig. 4A). On the other hand, at a radiation dose of 2 Gy, the proliferation and colony-forming ability of the cells were markedly reduced across all three treatments compared to the control group. The HfO_2NP and SAHA combined treatment led to the lowest number of colonies, fewer than in the samples treated with HfO_2NP or SAHA alone. In samples exposed to a radiation dose of 4 Gy, the SAHA treatment did not trigger a reduction of colony numbers compared to the control cells; however, we observed a notable attenuation in colony formation both following the nanoparticle as well as the HfO_2NP + SAHA exposures, the latter was significantly lower than the control, or the individual SAHA, or HfO_2NP treatments (Fig. 4A).

In the case of the MCF-7 cell line, the non-irradiated samples exhibited no differences in their colony-forming ability (Fig. 4B). When exposed to a radiation dose of 2 Gy, neither SAHA nor HfO_2NP demonstrated a significant effect compared to the control. However, the combination of SAHA and HfO_2NP resulted in a significant reduction in the number of colonies formed. This trend was also observed in samples irradiated with a 4 Gy dose. In this case, while either SAHA or the nanoparticles alone did not significantly decrease the colony-forming ability of MCF-7 cells compared to the control, the two agents together could massively inhibit the proliferation and colony formation (Fig. 4B).

A critical consideration in the development of combination therapies is whether the observed cytotoxic and radiosensitizing effects of SAHA and HfO_2NP combination are selectively exerted on malignant cells or if similar responses are expected in non-cancerous cells as well. To address this issue, we performed parallel experiments using MRC-5 non-cancerous human lung fibroblasts, employing the same treatment conditions as on cancer cell lines. Our results demonstrate that none of the treatments, whether with or without irradiation, SAHA, or HfO_2NPs alone or in combination, significantly compromised the viability of fibroblasts (Fig. S4A). Furthermore, lactate dehydrogenase (LDH) release assays revealed no cytotoxicity in response to any of the treatment conditions on non-cancerous cells (Fig. S4B). Accordingly, clonogenic assays were also executed, and these showed no significant reduction in the colony-forming abilities of MRC-5 cells following exposure to SAHA, HfO_2NP, or HfO_2NP + SAHA in the presence of 4 Gy irradiation (Fig. S4C). Therefore, our findings suggest that the cytotoxic and radiosensitizing effects of hafnium oxide nanoparticles in combination with the HDAC inhibitor SAHA are specific to cancer cells and do not adversely affect non-cancerous fibroblast cells, highlighting the therapeutic selectivity of the SAHA + HfO_2NP combination.

HfO_2NP treatment in combination with the HDAC inhibitor SAHA induces oxidative stress in tumor cells

To elucidate the mechanistic basis of the enhanced cytotoxic and radiosensitizing features observed with the combination of hafnium oxide nanoparticles and HDAC inhibitor SAHA across the tested cancer cell lines, we conducted a comprehensive analysis of key cellular stress and damage pathways. Specifically, we investigated the capacity of the treatments to induce oxidative stress, damage the DNA and mitochondria, trigger endoplasmic reticulum stress, and activate apoptotic signalling pathways. These mechanistic insights help to clarify the molecular basis of the observed therapeutic synergy.

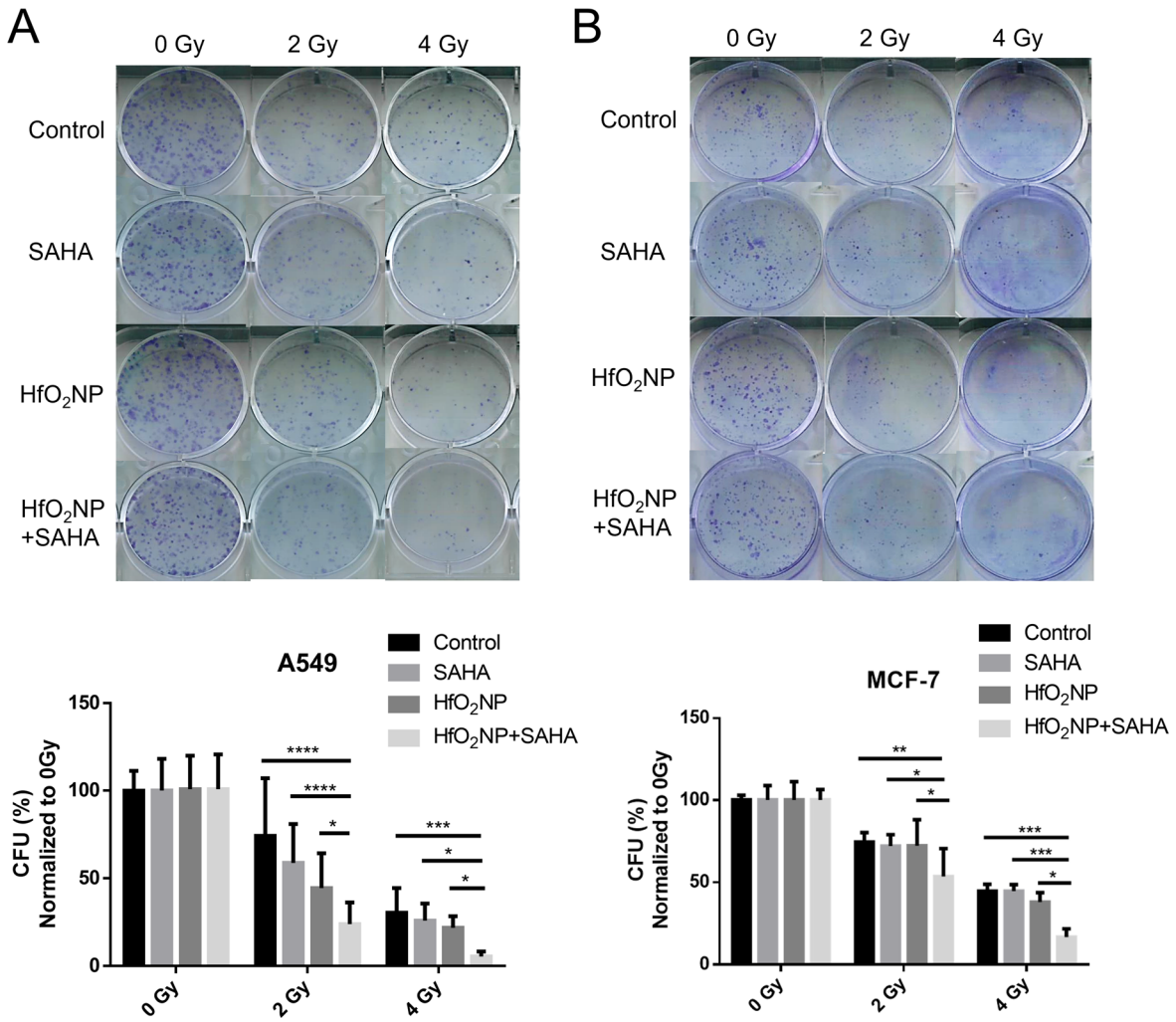

Fig. 4 The colony-forming performance of cancer cells following chemo- and radiation treatment. HfO_2NP, SAHA, and their combination significantly decreased the colony-forming ability of A549 cells (A) and MCF-7 cells (B) upon ionizing radiation. Two-way ANOVA, Tukey's multiple comparisons test, ****$P < 0.0001$, ***$P < 0.0005$, **$P < 0.005$, *$P < 0.05$.

For this aim, first, we performed a DCFDA staining to assess whether HfO_2NPs, SAHA, or their combination, together with ionizing radiation, enhance the production of reactive oxygen species (ROS) in tumor cells (Fig. 5). In the A549 cell line, treatments with any of the agents in the absence of irradiation did not result in an increase in ROS levels compared to untreated controls (Fig. 5A). Upon exposure to a dose of 2 Gy ionizing radiation, either SAHA or HfO_2NPs alone did not enhance ROS production significantly, however, the combined treatment with SAHA and HfO_2NPs under irradiation induced a pronounced increase in ROS levels, surpassing those obtained in both the irradiated control and the groups receiving individual treatments (Fig. 5A).

Similar results were gathered from the experiments on the MCF-7 cell line after 2 Gy irradiation. However, in this case, already at 0 Gy dose, the SAHA and HfO_2NPs combination proved to trigger significant ROS generation compared to individual drug treatments and control cells (Fig. 5B). Based on this, it was not surprising that samples subjected to SAHA and HfO_2NPs, as well as to 2 Gy radiation dose, induced similarly the formation of substantial amounts of reactive oxygen species.

These findings imply that the combination of SAHA and HfO_2NPs effectively enhances intracellular ROS levels in both cell lines.

The HfO_2NP treatment significantly enhances the DNA-damaging effect of ionizing radiation

To assess the extent of DNA damage induced by the treatments, we conducted immunofluorescent staining for γ-H2AX, a well-established marker of DNA double-strand breaks. Quantitative analysis included determining the proportion of γ-H2AX-positive cells in the samples within each treatment group, as well as quantifying the number of γ-H2AX foci per nucleus, to evaluate the frequency and severity of the DNA double-strand breaks at the single-cell level (Fig. 6).

In the case of non-irradiated A549 cells, we observed no increase in the number of γ-H2AX-positive cells compared to the control group, regardless of the treatment applied. However, in samples exposed to the combination of SAHA and HfO_2NP

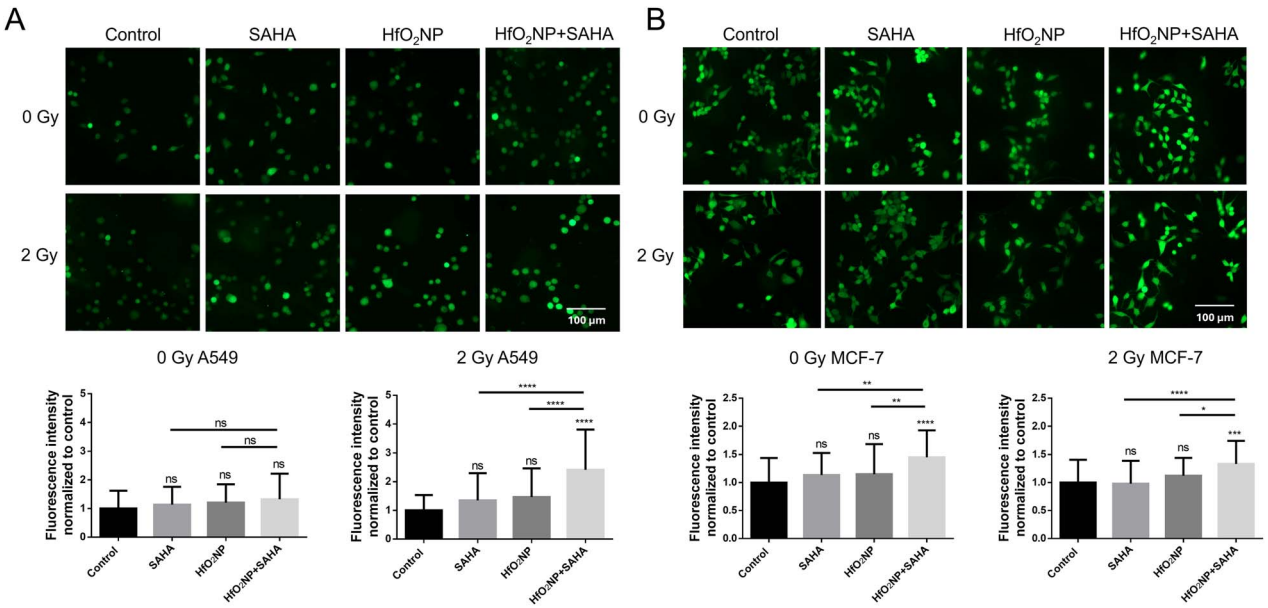

Fig. 5 The degree of oxidative stress induced by hafnium oxide nanoparticles, SAHA and ionizing radiation in cancer cells. The combination of HfO_2NP and SAHA significantly increases the level of reactive oxygen species upon ionizing radiation in A549 cells (A) and in MCF-7 cells (B). One-way ANOVA, Tukey's multiple comparisons test, ****$P < 0.0001$, ***$P < 0.0005$, **$P < 0.01$, *$P < 0.05$. Scale bar: 100 µm.

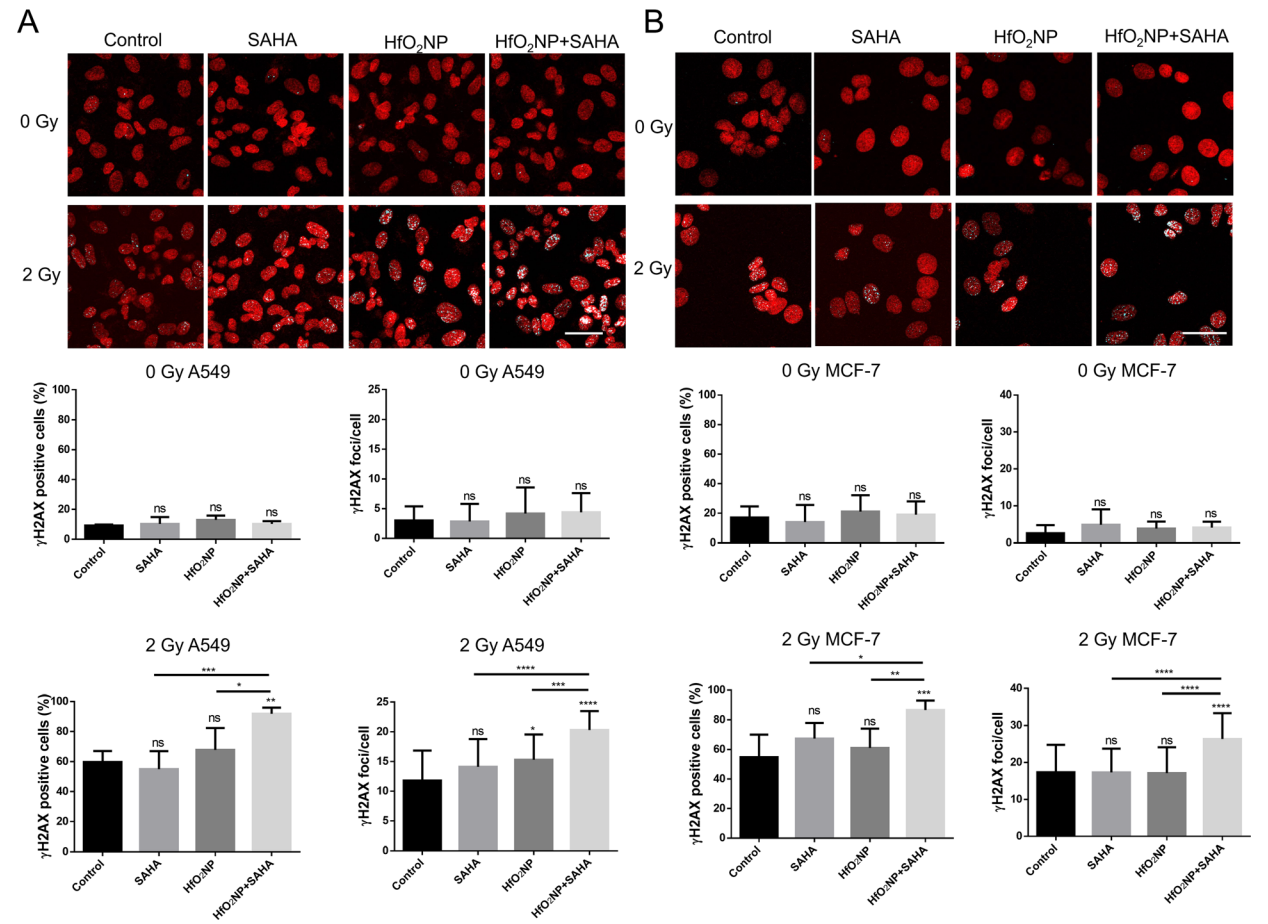

Fig. 6 The extent of DNA damage induced by hafnium oxide nanoparticles, SAHA, and ionizing radiation in cancer cells. The combination of HfO_2NP and SAHA significantly increases the amount of DNA double-strand breaks upon ionizing radiation in A549 (A) and in MCF-7 cells (B). One-way ANOVA, Tukey's multiple comparisons test, ****$P < 0.0001$, ***$P < 0.0005$, **$P < 0.005$, *$P < 0.05$. Scale bar 50 µm.

subjected to a 2 Gy radiation dose, there was a significant increase in the number of γ-H2AX-positive cells compared not only to the control but also to individual SAHA or HfO_2NP treatments (Fig. 6A). Regarding the number of intracellular γ-H2AX foci, we found no differences between the treatments in the non-irradiated samples, similarly to the results on γ-H2AX-positive cells. However, in samples exposed to irradiation, HfO_2NP administration led to an increase in the number of intracellular foci. Notably, the combination of SAHA and HfO_2NP resulted in a significant enhancement in the number of DNA double-strand breaks within cells when compared to the control and the individual treatments (Fig. 6A).

Regarding MCF-7 cells (Fig. 6B), there was no detectable difference in the number of γ-H2AX-positive cells between the individual treatments in the 0 Gy samples. However, in samples exposed to a radiation dose of 2 Gy, the combination treatment of SAHA and HfO_2NP resulted in a significant increase in the number of γ-H2AX-positive cells. Analysing the intracellular γ-H2AX foci, no significant rise in their number was observed upon either treatment when the samples were not irradiated. Conversely, in the irradiated cells, the incidence of intracellular DNA double-strand breaks increased significantly following the SAHA and HfO_2NP treatment (Fig. 6B).

Overall, our results suggest that without any irradiation, the treatments with either SAHA or HfO_2NP alone or their combination do not induce DNA damage; however, when ionizing radiation is also applied, the combination of the nanoparticle and the HDAC inhibitor enhances not simply the number of γ-H2AX-positive cells but also the number of DNA damage foci within the cells.

Treatments with HfO_2NP individually and in combination with SAHA significantly damage the mitochondria and trigger apoptosis

To assess the mitochondrial-damaging effects of the treatments, JC-1 staining was performed, and the resulting images were analyzed using ImageJ software (Fig. 7). In unhealthy or apoptotic cells due to an increased membrane permeability and consequent loss of electrochemical potential, JC-1 retains more of its original green fluorescence; thus, a reduction in the red-to-green fluorescence intensity ratio is characteristic of mitochondrial depolarization resulting from the applied treatments.

In the case of the A549 cell line, the mitochondrial-damaging effects of the treatments were evident even in the non-irradiated samples. When compared to the control and SAHA-treated samples, both HfO_2NP and the HfO_2NP and SAHA combination treatment significantly reduced the intensity of the red/green fluorescent signal. In samples exposed to a radiation dose of 2 Gy, SAHA exposure again did not induce a significant difference in mitochondrial membrane potential compared to

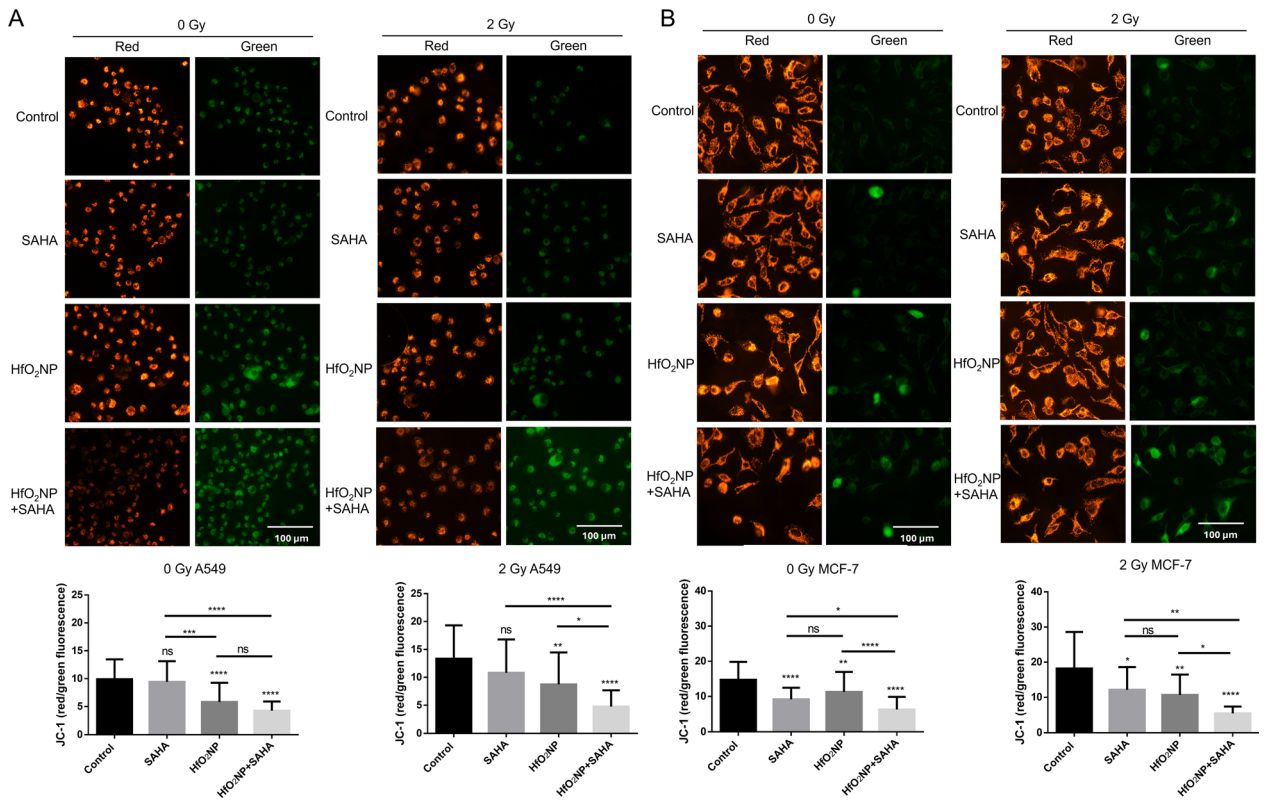

Fig. 7 The grade of mitochondrial damage induced by hafnium oxide nanoparticles, SAHA, and ionizing radiation in cancer cells. HfO_2NP and the combination of HfO_2NP and SAHA induce significant loss of mitochondrial membrane potential in A549 cells (A). In MCF-7 cells, HfO_2NP, SAHA, as well as their combination led to mitochondrial membrane depolarization (B). One-way ANOVA, Tukey's multiple comparisons test, ****P < 0.0001, ***P < 0.0005, **P < 0.005, *P < 0.05. Scale bar: 100 µm.

the control, while HfO_2NP triggered a marked decrease in red/green fluorescent ratio. The most prominent effect was observed with the HfO_2NP and SAHA combination treatment, which led to a substantially reduced red/green intensity signal compared to the other conditions (Fig. 7A).

For the MCF-7 cell line, we observed that all three treatments induced mitochondrial dysfunction in the non-irradiated cells compared to the control. Notably, the HfO_2NP and SAHA combination treatments led to a significant decrease in the intensity of the red/green fluorescent signal compared to the individual treatments. In irradiated samples, all three treatments induced mitochondrial damage; however, the combination treatment again exhibited the most pronounced effect. Administration of HfO_2NP + SAHA led to a significant reduction in the intensity of the red/green fluorescent signal compared to the control, SAHA, and HfO_2NP samples (Fig. 7B).

Based on the above-described observations, it seems plausible that HfO_2NPs, as well as the HDAC inhibitor, have the potential to induce mitochondrial dysfunction, but their combination has the most significant impact on the mitochondrial membrane potential, a feature that is maintained when cells are exposed to high-energy ionizing radiation.

We found so far that the treatments resulted in oxidative stress, generating a massive amount of reactive oxygen species, which in turn would target biomolecules and cellular organelles, thereby inducing DNA damage, genotoxic lesions, membrane disorder, and disruption of mitochondrial membrane potential. It is known that oxidative stress and disrupted calcium homeostasis can induce endoplasmic reticulum (ER) stress, activating the unfolded protein response (UPR), which might end in apoptosis if the restoration of ER function is no longer possible. Impaired mitochondrial function itself can trigger the release of various pro-apoptotic factors, leading to compromised cell survival and converging to the apoptotic cell death pathway in cancer cells.

For this aim, we investigated the possibility of ER stress and UPR induction in A549 and MCF-7 cells exposed to SAHA, HfO_2NPs, or their combination, followed by irradiation. We selected 8 different marker genes, namely binding immunoglobulin protein (BiP), C/EBP homologous protein (CHOP), activating transcription factor 4 (ATF4), ER degradation-enhancing alpha-mannosidase-like protein (EDEM), activating transcription factor 6 (ATF6), heat shock protein 90 kDa beta member 1 (GRP94, also known as endoplasmin), and X-box binding protein 1 (XBP1), including both segmented (XBP1s) and total forms (XBP1t), and their expression was assessed by qPCR. Our results revealed no signs of ER stress or UPR triggered by the agents and the ionizing radiation in the tested cancer cell lines, suggesting that ER stress is not inherently involved in the molecular mechanism of the enhanced cytotoxic and radiosensitizing features and the therapeutic synergy of SAHA and hafnium oxide nanoparticles (Fig. S5 and S6).

To examine whether the treatments and the irradiation together induce apoptosis in the subjected cancer cells, a caspase-3/7 activity assay was performed (Fig. 8). Although MCF-7 cells are known to lack functional caspase-3 due to a deletion in the corresponding gene, caspase activity assays targeting other caspases – particularly executioner caspases such as caspase-7 – can still provide meaningful results about the apoptotic signalling in this cell line. In both A549 and MCF-7 cells, significantly higher caspase-3/7 activity was measured upon treatments with HfO_2NPs, or with the combination of HfO_2NPs and SAHA after 2 Gy irradiation (Fig. 8). The individual SAHA treatment induced only a mild induction of apoptosis in these cells. Importantly, the highest caspase-3/7 enzyme activity was detected in the HfO_2NP + SAHA-treated cells, both in A549 as well as in MCF-7 cells. Therefore, the activation of apoptotic signalling pathways is indeed an essential part of the molecular mechanism behind the augmented radiosensitizing effects of the nanoparticle – SAHA combination across the tested cancer cell lines.

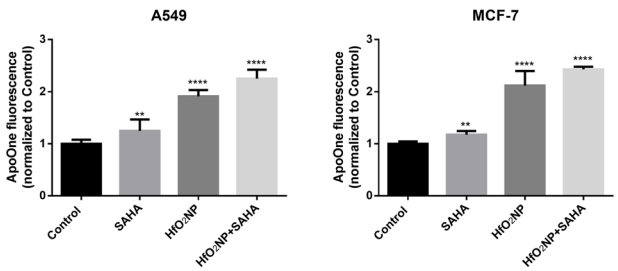

Fig. 8 Apoptosis induction based on the activity of executioner caspases in irradiated cancer cells pretreated with SAHA, hafnium oxide nanoparticles, and their combination after 2 Gy irradiation. The HfO_2NP, SAHA, and their combination induce apoptosis in A549 cells and MCF-7 cells upon ionizing radiation. Two-way ANOVA, Dunnett's multiple comparisons test, ****$P < 0.0001$, **$P < 0.01$.

The combination of HfO_2NP and SAHA significantly reduces the colony-forming capacity of cancer cells in 3D spheroids

While conventional 2D cell cultures are widely used models for investigating how tumor cells react to anti-cancer treatment modalities, they offer only a partial representation of an *in vivo* tumor microenvironment, particularly regarding structural complexity, physiological drug penetration barriers, and radiation response of solid tumors. To complement our findings and improve their physiological relevance, we expanded our investigation to include 3D spheroid models as well.

For this aim, colony formation assays were carried out using homotypic tumor spheroids to better estimate the impact of treatments on the division of cells within a 3-dimensional tumor model. Spheroids received individual SAHA, HfO_2NP, and also HfO_2NP + SAHA combinations as well as radiation treatment in the 3D form, then the spheroids were converted to single cell suspensions, and the samples were prepared for clonogenic assay, similarly to the original 2D cultures (Fig. 9). In the case of the irradiated A549 spheroids, either SAHA or the nanoparticles applied alone did not lead to a significantly reduced colony-forming ability of the cells (Fig. 9A). However, as expected, the combination of HfO_2NP + SAHA resulted in a notable decrease in both adhesion and division capabilities of the cells compared to the control, SAHA, and HfO_2NP treatments (Fig. 9A).

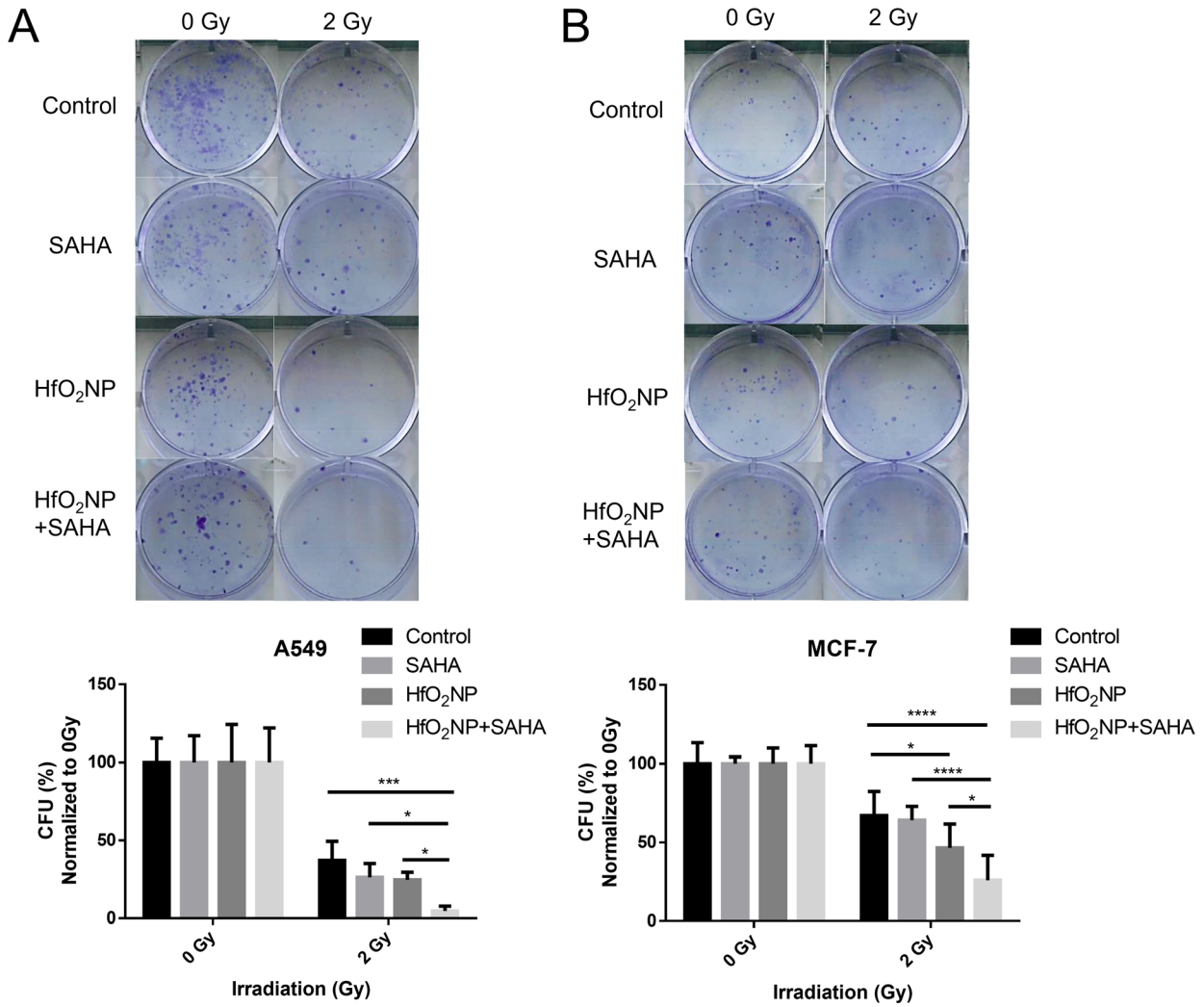

Fig. 9 The HfO_2NP, SAHA, and their combination significantly decreased the colony-forming ability of A549 cells (A) and MCF-7 cells (B) grown in 3D cell cultures upon ionizing radiation. Two-way ANOVA, Tukey's multiple comparisons test, ****$P < 0.0001$, ***$P = 0.0001$, *$P < 0.05$.

The colony-forming ability of MCF-7 cells within the spheroids exposed to the nanoparticles, either alone or in combination with the HDAC inhibitor, significantly diminished following irradiation with a 2 Gy dose. On the other hand, exposure of spheroids to SAHA and irradiation did not result in a statistically meaningful difference in colony-forming ability of these cells (Fig. 9B). Importantly, as anticipated, the HfO_2NP + SAHA combination treatment, together with ionizing radiation, significantly decreased the number of colonies initiated from these cells compared to individual SAHA or HfO_2NP administration (Fig. 9B). We can therefore prove that the SAHA-complemented, HfO_2NP-mediated enhanced cellular effects of irradiation manifest also in 3D spheroids, validating further the synergistic concept of hafnium oxide nanoparticles and HDAC inhibitors upon irradiation.

Discussion

Radiation therapy is a cornerstone of modern oncologic care, employed in the management of more than half of all cancer patients either as a definitive treatment, as an adjuvant modality, or for palliation. Technological innovations of the last decade, with state-of-the-art modalities such as intensity-modulated, image-guided, stereotactic body radiotherapy as well as proton therapy, have improved the accuracy of dose delivery, enabling higher precision in subjecting tumor tissues to ionizing radiation and enhancing tumor eradication.[34] Although these developments can ameliorate the tumor-targeting efficacy, damage to the surrounding healthy tissues by high-energy ionizing radiation cannot be completely eliminated. To attenuate further and minimize the collateral damage of healthy tissues, radiosensitizing agents can be utilized. Another challenge to face is the inherent or acquired radioresistance which is often noticed in certain breast, non-small cell lung, and androgen-independent prostate cancers. To overcome such radioresistance without continuously increasing the irradiation dose could be realized by the administration of radiosensitizers. These molecules enhance the susceptibility of cancer cells to ionizing radiation, improve tumor control while allowing for lower radiation doses. As research advances, novel

radiosensitizers and combination regimens aim to further improve the therapeutic ratio, offering the possibility of more effective, personalized, and less toxic cancer treatments.[35,36] A key principle in designing radiosensitizing combinations, is to identify the lowest drug concentration that preserves biological activity yet produces the strongest radiation-dependent therapeutic gain, since the primary therapeutic benefit is intended to arise only upon exposure to ionizing radiation. Among the various agents explored for this purpose, hafnium oxide nanoparticles have gained considerable attention. Compared to other high-Z nanoparticles, HfO_2NPs possess a combination of advantageous traits such as chemical stability under physiological conditions, low inherent toxicity, clinical readiness, evidenced by ongoing trials with the NBTXR3. This formulation contains phosphate-functionalized, 50 nm-sized HfO_2NPs, for intratumoral administration before radiotherapy, with early-phase clinical trials demonstrating its safety and tolerability.[11,37,38] While the promise of HfO_2NPs is substantial, challenges such as optimization of delivery methods, patient selection strategies, and integration with multimodal therapies, including chemotherapy and combinational modalities, need to be thoroughly investigated before widespread adoption. Building on this evidence, we designed this present investigation on the radiosensitization potential of HfO_2NPs in combination with the HDAC inhibitor SAHA across various cancer models, with a particular focus on elucidating underlying mechanisms and assessing translational relevance in both 2D and 3D tumor systems. We have selected A549 cells as one of the model systems to represent typical radioresistant cancer types, in order to examine whether these challenging tumors could be efficiently eliminated by radiotherapy combined with HfO_2NPs and SAHA exposures.

For effective anti-tumor applications, nanoparticles must be delivered to tumor cells with high efficiency and selectivity to maximize therapeutic effects and minimize off-target actions. Once in the tumor mass, in the vicinity of cancer cells, nanoparticles can be internalized by these cells through a variety of active uptake mechanisms, including clathrin-mediated or caveolin-mediated endocytosis, phagocytosis, and micropinocytosis. The predominant pathway is strongly influenced by both intrinsic properties of the nanoparticles, like size, surface charge, morphology, and functionalization, and also by some characteristics specific to the particular malignant cell type, such as receptor expression profiles, metabolism, membrane composition, and cell surface charge.[39–45] Beyond these physicochemical determinants, certain features of the tumor microenvironment also play a critical role in nanoparticle uptake. These are extracellular matrix composition and density, vascular permeability, interstitial fluid pressure, and 3D structure of the tumor, just naming a few.[46] In the context of radiotherapy, the efficient intracellular accumulation of the nanoparticles is a prerequisite for maximizing the radiosensitizing effect of these agents in order to achieve selective delivery and potent dose amplification.

On these grounds, an imperative and essential point of our study was to examine whether hafnium oxide nanoparticles are effectively taken up by the cancer cell models selected for investigation. Our analysis confirmed that, in fact, both A549 lung adenocarcinoma and MCF-7 breast carcinoma cells can readily internalize and accumulate HfO_2NPs to a substantial degree, with predominant localization in the cytoplasmic compartment, likely within endo-lysosomal vesicles. Intracellularly accumulated high-Z metal-based nanoparticles provide an electron-dense platform for the generation of reactive electrons, which in turn induce the localized bursts of ROS formation predominantly through water radiolysis, resulting in oxidative stress, which altogether promotes the oxidative damage to nucleic acids, membrane lipids, proteins, and various cellular organelles. If not effectively repaired, these macromolecular and structural injuries can trigger intrinsic apoptotic pathways.[47] In addition to a direct radiosensitization, hafnium-based nanoparticles, such as NBTXR3, have been reported to exert immunomodulatory effects. Lysosomal membrane permeabilization following nanoparticle uptake and irradiation has been linked to the induction of immunogenic cell death, where the released damage-associated molecular patterns (DAMPs) activate antigen-presenting cells and enhance anti-tumor immunity. Moreover, HfO_2NPs were implicated in inducing ferroptosis, the iron-dependent form of cell death, as well, adding another layer to their molecular actions.[48,49]

To further improve the anti-tumor efficacy of radiotherapy, nanoparticles can be administered in combination with other therapeutic agents that enhance the cytotoxic effects of ionizing radiation. Such combination strategies aim to exploit complementary mechanisms to induce additional molecular pathways leading to cancer cell death, thereby increasing the likelihood of malignant cell elimination. Radiosensitizing combinational agents might target and interfere with DNA repair, modulate hypoxia, or trigger further ROS generation to hinder tumor survival pathways. Histone-deacetylase inhibitors, which are already approved and applied in clinical settings for the treatment of certain hematopoietic malignancies and are under investigation for various solid tumors, can be suitable combinational and radiosensitizing partners of metal-based nanoparticles. By promoting hyperacetylation of the targeted histone and non-histone proteins, HDAC inhibitor treatments result in an increased chromatin relaxation, thereby enhancing DNA accessibility to the DNA-damaging effects of ionizing radiation and reactive oxygen species.[31,50] HDAC inhibitors can also impair the expression and function of key DNA repair proteins, interfere with cell cycle progression, induce apoptosis in tumor cells *via* the increased acetylation state of key proteins, such as p53, trigger autophagy, and increase the level of ROS, all of which synergize with the localized energy deposition mediated by HfO_2NPs.[51,52]

Therefore, we hypothesized that combining high-Z metal-based nanoparticles with HDAC inhibitors offers the possibility of a dual radiosensitization strategy, where the physical phase of dose enhancement with secondary electron emission from the HfO_2NPs and the biological component of the dose enhancement arising from the epigenetic modulation by HDAC inhibitors are competently and profitably coupled. Such an integrated approach enables an exceptional tumor control, which is particularly advantageous in radioresistant cancers. In

fact, we found that HfO_2NPs and the HDAC inhibitor SAHA efficiently radiosensitized tumor cells, the amount of intracellular ROS increased in both cell lines upon irradiation. For this particular experiment and also for further assays the concentration of 60 μg mL^{-1} of hafnium oxide nanoparticles was set, as this concentration ensured robust intracellular nanoparticle accumulation and maximal radiation-dependent enhancement of tumor cell killing, and at the same time avoiding direct cytotoxic effects. It is also noteworthy that in MCF-7 cells, the HfO_2NPs + SAHA combination significantly increased the level of ROS already without irradiation, indicating a chemosensitizing feature of their joint action on tumor cells prior to irradiation.

To investigate whether the production of massive amounts of reactive oxygen species induced structural and functional damage in macromolecules and cell organelles, we examined mitochondrial function, DNA damage, cell proliferation, colony formation, apoptosis as well as ER stress induction in the treated cancer cells.

Silver nanoparticles have previously been shown to induce cell death through the activation of endoplasmic reticulum stress pathways.[53,54] The ER is generally responsible for maintaining cellular homeostasis by regulating calcium ion storage, sustaining redox balance, and ensuring proper protein folding. Perturbations in ER function caused by oxidative or proteotoxic stress can lead to the accumulation of misfolded proteins, thereby triggering ER stress and eventually the unfolded protein response (UPR).[55,56] UPR serves as an adaptive mechanism aimed at restoring homeostasis by attenuating protein synthesis and upregulating ER chaperones; however, if ER stress is prolonged or severe, the UPR switches to a pro-apoptotic mode. Since ROS are key inducers of endoplasmic reticulum stress, ER stress may arise as a consequence of oxidative stress-inducing nanoparticle treatments.[57] Based on this rationale, we investigated whether HfO_2NPs alone or in combination with SAHA under ionizing radiation, could activate ER stress and UPR-related pathways in A549 and MCF-7 cells. For this, we quantified the mRNA expression of established ER stress and UPR marker genes. Our results demonstrated no biologically significant changes in the expression of most critical ER stress and UPR genes following HfO_2NPs, SAHA, and their combined treatments with irradiation (SI Fig. S5 and S6). Among the various markers, the only notable alteration was a statistically significant upregulation of Xbp1t gene in MCF-7 cells compared to the untreated control (SI Fig. S6). This gene encodes the transcriptionally active spliced form of X-box binding protein 1, a central regulator of the UPR. These findings indicate that under the tested experimental conditions, HfO_2NPs and SAHA combined with irradiation do not elicit pronounced ER stress response in these cancer cells, suggesting that the observed radiosensitizing effects are unlikely mediated *via* ER stress-driven cytotoxicity.

Mitochondria represent another subcellular target for metal-based nanoparticles, as well as HDAC inhibitors and ionizing radiation. Mitochondria are key organelles for energy production, redox homeostasis, and the regulation of apoptosis. One of the earliest indicators of mitochondrial distress is the loss of mitochondrial membrane potential, which is inherently associated with the activation of the intrinsic apoptotic pathways.[58–60] In our experiments, individual HfO_2NPs, or SAHA treatments, or their combination without irradiation resulted in a significant decrease in the mitochondrial membrane potential compared to the untreated samples. This depolarization of the mitochondrial membrane could be both a cause and a consequence of high ROS levels, since excessive ROS can damage mitochondrial membranes and the electron transport chain components, while mitochondrial dysfunction can also aggravate ROS generation, thereby producing a self-amplifying cycle of oxidative stress. Upon ionizing radiation, the HfO_2NP and SAHA in combination produced an even more pronounced decrease in the mitochondrial membrane potential compared to the irradiated untreated cells and to cells receiving either treatment alone. This synergistic depolarization under radiation implies that the combination treatment augments mitochondrial damage beyond the additive effects and implicitly also hints that such a degree of mitochondrial collapse would trigger pro-apoptotic signaling pathways but may also sensitize cancer cells to subsequent oxidative and genotoxic insults. Based on the above, mitochondria must be the central execution points of the cytotoxic actions of HfO_2NP and SAHA combinations under ionizing radiation.

Ionizing radiation primarily damages the cellular membrane structures and induces lesions in the DNA. Among these, the most dangerous DNA damage is the DNA double-strand break, as it disrupts the continuity of both strands and poses a substantial challenge to the correcting mechanisms. Cells try to repair these breaks by the homologous repair and the non-homologous end joining, the latter being a faster but more error-prone mechanism.[61] To quantify the extent of the DNA damage, more specifically of DNA double-strand breaks, we employed γ-H2AX immunostaining, a sensitive and widely utilized method to visualize double-strand breaks by detecting the phosphorylated form of the H2AX histone at these sites. Our quantification included not only the percentage of γ-H2AX-positive cells, but we also counted the number of γ-H2AX foci per nucleus, this way, we evaluated the frequency and the severity of the DNA damage. Our results showed that without irradiation, the treatments with either HfO_2NP or SAHA alone or their combination did not induce a measurable increase in DNA damage. This suggests that the HfO_2NPs and SAHA at the tested concentrations are unlikely to induce genotoxic effects, a very important issue regarding healthy cells and tissues, supporting the safety of HfO_2NPs. Nevertheless, when ionizing radiation is also applied, the combination of the nanoparticle and the HDAC inhibitor markedly amplifies DNA damage, evidenced by the remarkable increase in the number of γ-H2AX-positive cells and also the number of DNA damage foci within the cells. The potentiation of radiation-induced DNA double-strand breaks reflects both the physical components of radiosensitization involving HfO_2NPs, which generate reactive secondary electrons and ROS in the close proximity to DNA molecules. And also mirror the biological phase of radiosensitization executed by SAHA, promoting chromatin relaxation and inhibiting DNA

repair by epigenetic mechanisms, thereby increasing the persistence of ionizing radiation-induced DNA damage.

Our results demonstrate that both HfO_2 nanoparticles and the HDAC inhibitor individually have the capacity to induce oxidative stress and disrupt mitochondrial homeostasis; however, when administered in combination, these agents exerted the most pronounced effects, pointing toward a synergistic interaction. This enhancement was observed under baseline conditions (without irradiation) but was even further amplified when ionizing radiation was also applied. This implies that the HfO_2NPs and SAHA combined treatment installs an increased susceptibility of mitochondria to radiation-induced injury, establishing thereby a clear mechanistic link between oxidative stress induction, mitochondrial dysfunction, and the potentiation of DNA damage in the radiosensitization effect of the HfO_2NPs and SAHA combination.

Mitochondrial dysfunction, oxidative stress, and persistent DNA damage are all critical determinants of the cellular decision to commit to apoptosis. From the damaged mitochondria, a range of pro-apoptotic factors are released into the cytosol to initiate caspase-dependent and independent cell death pathways. Such a factor is cytochrome c, which activates the initiator caspase-9, this in turn triggers the executioner caspases, particularly caspase-3 and caspase-7, culminating in the proteolytic decay of structural and regulatory proteins.[62–64] In this study, we proved by quantitative assays that the nanoparticle treatments in combination with HDAC inhibitor exposure and irradiation led to a substantial increase in apoptosis, confirming that the observed mitochondrial and DNA damage translates into the activation of programmed cell death pathways.

Although identifying the predominant pathway of nanoparticle uptake into cancer cells was beyond the scope of the present study, from a mechanistic and functional perspective, the exact route of entry is unlikely to critically influence the radiosensitizing efficacy of the HfO_2NPs + SAHA combination examined here. The key prerequisite for physical dose enhancement is the intracellular presence and retention of high-Z material, rather than the specific vesicular pathway through which the nanoparticles enter the cell. Nevertheless, uptake-pathway-specific studies would be highly valuable for a comprehensive nanobiological characterization and represent an important direction for future research.

Finally, to assess the functional consequences of the combined nanoparticle and HDAC inhibitor treatment on long-term tumor survival, cell proliferation, and colony-forming ability, we performed clonogenic assays on 2D monolayer cultures and 3D tumor spheroid models. Our results verified that the combination of HfO_2NPs, SAHA, and ionizing radiation produced a marked and statistically significant reduction in the proliferation of tumor cells and their ability to form colonies in 2D and 3D models compared to single-agent treatments. It looks like that the radio- and chemosensitizing effects of the HfO_2NPs + SAHA combination are quite robust and realize into profound impairment of long-term survival and serious incapacitation of the tumor cells to regrow. The inclusion of 3D tumor spheroids in the study is particularly relevant as these models imitate more closely the *in vivo* environment than 2D cultures. Spheroids exhibit physiologically appropriate gradients of nutrients, oxygen, pH, and metabolic activity, and also some structural characteristics such as a hypoxic core and proliferative surface, diffusion, and cellular heterogeneity, more adequately resembling the architectural and metabolic situations in tumors. Moreover, these listed characteristics significantly influence the drug penetration, the distribution of the radiation dose, and affect also cellular responses, providing a more realistic predictive platform to evaluate the efficiency of a given treatment approach. As we demonstrate here that the HfO_2NPs + SAHA combination, together with irradiation, is effective on 3D spheroids, we provide evidence that its therapeutic potential can be extended to more complex, tumor-like microenvironments, which strengthens the translational value of this particular multimodal combination. Importantly, as we found no major differences between the behavior and the effects of HfO_2NPs, SAHA together with irradiation on A549 and MCF-7 cells, these data also indicate that this combination exerts potent cytotoxic effects in both intrinsically radiosensitive and radioresistant cancer cell models. Thus, integration of physical dose amplification from high-Z nanoparticles with biological sensitization by HDAC inhibitors overcomes key resistance mechanisms. Consequently, this approach holds promise for targeting certain challenging, treatment-refractory radioresistant malignancies. It is also important to emphasize that HfO_2NPs, SAHA and their combination, with or without irradiation did not impair the viability or reduce the clonogenic survival in non-cancerous MRC-5 fibroblasts, indicating a lack of harmful effects on healthy cells under the tested conditions. This cancer-selective action is likely attributable to the preferential accumulation of nanoparticles in tumor tissues and to a larger susceptibility of malignant cells to oxidative and genotoxic stress. Such a tumor-specific sensitization is highly advantageous in radiotherapy as well as in any oncotherapeutic treatment approach.

Based on these data, a comprehensive mechanistic framework emerges behind the radiosensitizing effect of HfO_2NPs and SAHA. HfO_2NPs are taken up by tumor cells, where they accumulate in the cytosol. Histone deacetylase inhibitors also enter the cell, and *via* their action on HDAC enzymes and acetylated histone proteins, a highly relaxed chromatin structure is maintained. The HfO_2NPs, in combination with HDAC inhibitors, induce mitochondrial dysfunction and increase the level of intracellular reactive oxygen species. Upon ionizing radiation, the production of reactive electrons and reactive oxygen species is further amplified, mitochondrial dysfunction and DNA damage become even more profound, culminating in apoptosis, and a radical impairment in long-term cancer cell survival and regrowth. The fact that the combination retains its high efficacy in 3D model highlights its potential in a next-generation therapeutic approach for radioenhancement in clinical settings but also to overcome the challenges of microenvironment-mediated treatment resistance. Based on this and previous studies of our laboratory,[31,32] it is plausible that the concept presented here is inherently modular and extensible. The strategy combines a clinically relevant high-Z

nanoparticle platform and a clinically approved epigenetic radiosensitizer. This dual-mode radiosensitization approach is not restricted to SAHA or HfO_2NPs and could be extended to other HDAC inhibitors, alternative epigenetic modulators, different high-Z nanoparticle systems, and additional radiation-resistant tumor entities.

Conclusions

In this study, we demonstrate that the combination of hafnium oxide nanoparticles and the histone deacetylase inhibitor SAHA, when applied together with ionizing radiation, exerts a potent multimodal radiosensitizing action by a series of molecular and cellular mechanisms. This treatment induces massive oxidative stress, disrupts mitochondrial membrane potential, and amplifies radiation-induced DNA double-strand breaks. The effects culminate in the activation of apoptotic pathways, leading ultimately to a remarkable decrease in long-term clonogenic survival, manifested both in 2D and 3D tumor models. Importantly, this multimodal radiosensitizing approach maintained its efficacy against radiosensitive as well as radioresistant cancer cells, while exhibiting no adverse effects on non-cancerous MRC-5 fibroblasts, suggesting a high degree of tumor selectivity. The selective cytotoxicity, together with the capacity to overcome radioresistance, emphasizes the translational potential of this strategy. Thus, the integration of high-Z nanoparticle-mediated physical dose enhancement with HDAC inhibitor-driven biological radiosensitization offers a tumor-selective method to improve radiotherapy outcomes even in cases of the most challenging malignancies. Such novel combination regimens of high-Z metal-based nanosystems and HDAC inhibitors represent a highly versatile platform for next-generation radiosensitizing nanomedicines that can be exploited to reduce cancer cell growth and advance the therapeutic outcomes.

Author contributions

N. I., M. K. designed the project; C. B., N. I., K. S., D. I. A., E. R. S., R. P., B. P., A. R., and T. S. carried out the methodology; software analysis C. B., A. R., N. I.; formal analysis was carried out by C. B., N. I., and M. K.; data curation, N. I., R. P., T. S., Z. K., and K. H.; writing – original draft Preparation, C. B., N. I. and M. K.; writing & editing, N. I., K. S, B. P., E. R. S., K. H., C. B., Z. K. M., K.; funding acquisition, N. I., M. K., all authors reviewed the manuscript.

Conflicts of interest

The authors report no conflicts of interest in this work.

Data availability

All original data of this manuscript are available on request.

The supporting data has been provided as part of the supplementary information (SI). Supplementary information: Table 1, Fig. S1–S6. See DOI: https://doi.org/10.1039/d5na00845j.

Acknowledgements

The project was supported by the Incubation Competence Centre of the Centre of Excellence for Interdisciplinary Research, Development and Innovation of the University of Szeged (N. I. is the member of Molecular mechanisms of nanoparticle-induced radiosensitization research group) and the OTKA-NKFIH (K142371) and OTKA-NKFIH (PD143320) grants from the National Research, Development, and Innovation Office of the Hungarian Government. N. I. was supported by the János Bolyai Research Fellowship of the Hungarian Academy of Sciences (BO/00351/22/8), by the New National Excellence Program of the Ministry of Human Capacities of Hungary (ÚNKP-22-5-SZTE-553 and ÚNKP-23-5-SZTE-680), and by the University Research Scholarship Program of the Ministry for Culture and Innovation from the source of the National Research, Development and Innovation Fund (EKÖP-24-4-SZTE-626 for N. I.). D. A. was supported by the NTP-NFTÖ-22-B-0100 and NTP-NFTÖ-21-B-0157 grants of the National Excellence Program of the Ministry of Human Resources. The samples were irradiated in ELI-ALPS. ELI ALPS project (GINOP-2.3.6-15-2015-00001) is supported by the European Union and co-financed by the European Regional Development Fund.

References

1 R. Baskar, K. A. Lee, R. Yeo and K. W. Yeoh, Cancer and radiation therapy: current advances and future directions, *Int. J. Med. Sci.*, 2012, **9**(3), 193–199.
2 E. J. Moding, M. B. Kastan and D. G. Kirsch, Strategies for optimizing the response of cancer and normal tissues to radiation, *Nat. Rev. Drug Discov.*, 2013, **12**(7), 526–542.
3 W. C. Dewey, C. C. Ling and R. E. Meyn, Radiation-induced apoptosis: Relevance to radiotherapy, *Int. J. Radiat. Oncol. Biol. Phys.*, 1995, **33**(4), 781–796.
4 S. Bayda, M. Hadla, S. Palazzolo, P. Riello, G. Corona, G. Toffoli, *et al.*, Inorganic Nanoparticles for Cancer Therapy: A Transition from Lab to Clinic, *Curr. Med. Chem.*, 2018, **25**(34), 4269–4303.
5 H. Sharma, P. K. Mishra, S. Talegaonkar and B. Vaidya, Metal nanoparticles: a theranostic nanotool against cancer, *Drug Discov. Today*, 2015, **20**(9), 1143–1151.
6 Y. Liu, P. Zhang, F. Li, X. Jin, J. Li, W. Chen, *et al.*, Metal-based *NanoEnhancers* for Future Radiotherapy: Radiosensitizing and Synergistic Effects on Tumor Cells, *Theranostics*, 2018, **8**(7), 1824–1849.
7 N. Chattopadhyay, Z. Cai, J. P. Pignol, B. Keller, E. Lechtman, R. Bendayan, *et al.*, Design and Characterization of HER-2-Targeted Gold Nanoparticles for Enhanced X-radiation Treatment of Locally Advanced Breast Cancer, *Mol. Pharm.*, 2010, **7**(6), 2194–2206.
8 S. Her, D. A. Jaffray and C. Allen, Gold nanoparticles for applications in cancer radiotherapy: Mechanisms and

recent advancements, *Adv. Drug Deliv. Rev.*, 2017, **109**, 84–101.
9 A. A. Sherstiuk, S. A. Tsymbal, A. F. Fakhardo, V. N. Morozov, E. F. Krivoshapkina, E. Hey-Hawkins, *et al.*, Hafnium Oxide-Based Nanoplatform for Combined Chemoradiotherapy, *ACS Biomater. Sci. Eng.*, 2021, 7(12), 5633–5641.
10 A. F. Fakhardo, E. I. Anastasova, S. R. Gabdullina, A. S. Solovyeva, V. B. Saparova, V. V. Chrishtop, *et al.*, Toxicity Patterns of Clinically Relevant Metal Oxide Nanoparticles, *ACS Appl. Bio Mater.*, 2019, **2**(10), 4427–4435.
11 P. Zhang, J. Marill, A. Darmon, A. N. Mohamed, B. Lu and S. Paris, NBTXR3 Radiotherapy-Activated Functionalized Hafnium Oxide Nanoparticles Show Efficient Antitumor Effects Across a Large Panel of Human Cancer Models, *Int. J. Nanomed.*, 2021, **16**, 2761–2773.
12 S. Bonvalot, C. Le Pechoux, T. De Baere, G. Kantor, X. Buy, E. Stoeckle, *et al.*, First-in-Human Study Testing a New Radioenhancer Using Nanoparticles (NBTXR3) Activated by Radiation Therapy in Patients with Locally Advanced Soft Tissue Sarcomas, *Clin. Cancer Res.*, 2017, **23**(4), 908–917.
13 N. Scher, S. Bonvalot, C. Le Tourneau, E. Chajon, C. Verry, J. Thariat, *et al.*, Review of clinical applications of radiation-enhancing nanoparticles, *Biotechnol. Rep.*, 2020, **28**, e00548.
14 X. Liem, T. de Baère, O. I. Vivar, T. Y. Seiwert, C. Shen, Z. Pápai, *et al.*, International guidelines for intratumoral and intranodal injection of NBTXR3 nanoparticles in head and neck cancers, *Head Neck*, 2024, **46**(6), 1253–1262.
15 A. F. Bagley, E. B. Ludmir, A. Maitra, B. D. Minsky, G. Li Smith, P. Das, *et al.*, NBTXR3, a first-in-class radioenhancer for pancreatic ductal adenocarcinoma: Report of first patient experience, *Clin. Transl. Radiat. Oncol.*, 2022, **33**, 66–69.
16 A. C. West and R. W. Johnstone, New and emerging HDAC inhibitors for cancer treatment, *J. Clin. Invest.*, 2014, **124**(1), 30–39.
17 M. J. Ramaiah, A. D. Tangutur and R. R. Manyam, Epigenetic modulation and understanding of HDAC inhibitors in cancer therapy, *Life Sci.*, 2021, **277**, 119504.
18 L. F. Fröhlich, M. Mrakovcic, C. Smole and K. Zatloukal, Molecular mechanism leading to SAHA-induced autophagy in tumor cells: evidence for a p53-dependent pathway, *Cancer Cell Int.*, 2016, **16**(1), 68.
19 M. V. Blagosklonny, S. Trostel, G. Kayastha, Z. N. Demidenko, L. T. Vassilev, L. Y. Romanova, *et al.*, Depletion of Mutant p53 and Cytotoxicity of Histone Deacetylase Inhibitors, *Cancer Res.*, 2005, **65**(16), 7386–7392.
20 D. Yin, J. M. Ong, J. Hu, J. C. Desmond, N. Kawamata, B. M. Konda, *et al.*, Suberoylanilide hydroxamic acid, a histone deacetylase inhibitor: Effects on gene expression and growth of glioma cells in vitro and in vivo, *Clin. Cancer Res.*, 2007, **13**(3), 1045–1052.
21 U. Natarajan, T. Venkatesan, V. Radhakrishnan, S. Samuel, P. Rasappan and A. Rathinavelu, Cell Cycle Arrest and Cytotoxic Effects of SAHA and RG7388 Mediated through p21WAF1/CIP1 and p27KIP1 in Cancer Cells, *Medicina*, 2019, **55**(2), 30.
22 A. Hrzenjak, M. Kremser, B. Strohmeier, F. Moinfar, K. Zatloukal and H. Denk, SAHA induces caspase-independent, autophagic cell death of endometrial stromal sarcoma cells by influencing the mTOR pathway, *J. Pathol.*, 2008, **216**(4), 495–504.
23 L. Liu, X. Sun, Y. Xie, Y. Zhuang, R. Yao and K. Xu, Anticancer effect of histone deacetylase inhibitor scriptaid as a single agent for hepatocellular carcinoma, *Biosci. Rep.*, 2018, **38**(4), BSR20180360.
24 J. A. Vrana, R. H. Decker, C. R. Johnson, Z. Wang, W. D. Jarvis, V. M. Richon, *et al.*, Induction of apoptosis in U937 human leukemia cells by suberoylanilide hydroxamic acid (SAHA) proceeds through pathways that are regulated by Bcl-2/Bcl-XL, c-Jun, and p21CIP1, but independent of p53, *Oncogene*, 1999, **18**(50), 7016–7025.
25 W. Wang, Y. Liu and L. Zhao, Tambulin Targets Histone Deacetylase 1 Inhibiting Cell Growth and Inducing Apoptosis in Human Lung Squamous Cell Carcinoma, *Front. Pharmacol*, 2020, **11**, 1188.
26 M. C. Chen, H. H. Huang, C. Y. Lai, Y. J. Lin, J. P. Liou, M. J. Lai, *et al.*, Novel histone deacetylase inhibitor MPT0G009 induces cell apoptosis and synergistic anticancer activity with tumor necrosis factor-related apoptosis-inducing ligand against human hepatocellular carcinoma, *Oncotarget*, 2016, **7**(1), 402–417.
27 M. J. Ramaiah, A. D. Tangutur and R. R. Manyam, Epigenetic modulation and understanding of HDAC inhibitors in cancer therapy, *Life Sci.*, 2021, **277**, 119504.
28 W. J. Huang, Y. A. Tang, M. Y. Chen, Y. J. Wang, F. H. Hu, T. W. Wang, *et al.*, A histone deacetylase inhibitor YCW1 with antitumor and antimetastasis properties enhances cisplatin activity against non-small cell lung cancer in preclinical studies, *Cancer Lett.*, 2014, **346**(1), 84–93, https://www.sciencedirect.com/science/article/abs/pii/S0304383513008410?via%3Dihub.
29 J. H. Lee, M. L. Choy, L. Ngo, S. S. Foster and P. A. Marks, Histone deacetylase inhibitor induces DNA damage, which normal but not transformed cells can repair, *Proc. Natl. Acad. Sci. U. S. A.*, 2010, **107**(33), 14639–14644.
30 F. Zhang, T. Zhang, Z. H. Teng, R. Zhang, J. B. Wang and Q. B. Mei, Sensitization to gamma-irradiation-induced cell cycle arrest and apoptosis by the histone deacetylase inhibitor trichostatin A in non-small cell lung cancer (NSCLC) cells, *Cancer Biol. Ther.*, 2009, **8**(9), 823–831.
31 N. Igaz, D. Kovács, Z. Rázga, Z. Kónya, I. M. Boros and M. Kiricsi, Modulating chromatin structure and DNA accessibility by deacetylase inhibition enhances the anti-cancer activity of silver nanoparticles, *Colloids Surf. B Biointerfaces*, 2016, **146**, 670–677.
32 N. Igaz, K. Szőke, D. Kovács, A. Buhala, Z. Varga, P. Bélteky, *et al.*, Synergistic Radiosensitization by Gold Nanoparticles and the Histone Deacetylase Inhibitor SAHA in 2D and 3D Cancer Cell Cultures, *Nanomaterials*, 2020, **10**(1), 158.
33 R. Polanek, Z. Varga, E. Fodor, Sz Brunner, E. R. Szabó, T. Tőkés, *et al.*, Improved FBX chemical dosimeter system with enhanced radiochemical yield for reference dosimetry

in radiobiology and radiotherapy research, *Radiat. Phys. Chem.*, 2020, **174**, 108899.
34 M. Webster, A. Podgorsak, F. Li, Y. Zhou, H. Jung, J. Yoon, *et al.*, New Approaches in Radiotherapy, *Cancers*, 2025, **17**(12), 1980.
35 L. Gong, Y. Zhang, C. Liu, M. Zhang and S. Han, Application of Radiosensitizers in Cancer Radiotherapy, *Int. J. Nanomed.*, 2021, **16**, 1083–1102.
36 J. Raviraj, V. Bokkasam, V. Kumar, U. Reddy and V. Suman, Radiosensitizers, radioprotectors, and radiation mitigators, *Indian J. Dent. Res.*, 2014, **25**(1), 83.
37 E. Vlastou, A. Kougioumtzopoulou, K. Platoni, I. Georgakopoulos, N. Lagopati, V. Kouloulias, *et al.*, The Emerging Role of Nanoparticles Combined with Either Radiotherapy or Hyperthermia in Head and Neck Cancer: A Current Review, *Cancers*, 2025, **17**(5), 899.
38 U. Schick, V. Bourbonne, F. Lucia and C. Verry, Use of nanoparticles in radiation oncology, *Cancer Radiother.*, 2024, **28**(6–7), 618–622.
39 S. Behzadi, V. Serpooshan, W. Tao, M. A. Hamaly, M. Y. Alkawareek, E. C. Dreaden, *et al.*, Cellular uptake of nanoparticles: journey inside the cell, *Chem. Soc. Rev.*, 2017, **46**(14), 4218–4244.
40 R. G. Parton and M. A. del Pozo, Caveolae as plasma membrane sensors, protectors and organizers, *Nat. Rev. Mol. Cell Biol.*, 2013, **14**(2), 98–112.
41 R. G. Parton and K. Simons, The multiple faces of caveolae, *Nat. Rev. Mol. Cell Biol.*, 2007, **8**(3), 185–194.
42 L. Hewlett, A. Prescott and C. Watts, The coated pit and macropinocytic pathways serve distinct endosome populations, *J. Cell Biol.*, 1994, **124**(5), 689–703.
43 J. A. Barreto, W. O'Malley, M. Kubeil, B. Graham, H. Stephan and L. Spiccia, Nanomaterials: Applications in Cancer Imaging and Therapy, *Adv. Mater.*, 2011, **23**(12), H18.
44 F. Alexis, P. Basto, E. Levy-Nissenbaum, A. F. Radovic-Moreno, L. Zhang, E. Pridgen, *et al.*, HER-2-Targeted Nanoparticle–Affibody Bioconjugates for Cancer Therapy, *ChemMedChem*, 2008, **3**(12), 1839–1843.
45 J. Mercer and A. Helenius, Virus entry by macropinocytosis, *Nat. Cell Biol.*, 2009, **11**(5), 510–520.
46 M. R. Dreher, W. Liu, C. R. Michelich, M. W. Dewhirst, F. Yuan and A. Chilkoti, Tumor Vascular Permeability, Accumulation, and Penetration of Macromolecular Drug Carriers, *JNCI (J. Natl. Cancer Inst.)*, 2006, **98**(5), 335–344.
47 S. Xiao, X. Wang, B. Chen, M. Mu, B. Han, N. Chen, *et al.*, Enhancing tumor radiotherapy sensitivity through metal nanomaterials: A comprehensive review, *Malig. Spectrum*, 2024, **1**(4), 243–262.
48 A. Darmon, P. Zhang, J. Marill, N. Mohamed Anesary, J. Da silva and S. Paris, Radiotherapy-activated NBTXR3 nanoparticles modulate cancer cell immunogenicity and TCR repertoire, *Cancer Cell Int.*, 2022, **22**(1), 208.
49 J. Da Silva, C. Bienassis, P. Schmitt, C. Berjaud, M. Guedj and S. Paris, Radiotherapy-activated NBTXR3 nanoparticles promote ferroptosis through induction of lysosomal membrane permeabilization, *J. Exp. Clin. Cancer Res.*, 2024, **43**(1), 11.
50 M. Q. Shi, Y. Xu, X. Fu, D. S. Pan, X. P. Lu, Y. Xiao, *et al.*, Advances in targeting histone deacetylase for treatment of solid tumors, *J. Hematol. Oncol.*, 2024, **17**(1), 37.
51 A. Drazic, L. M. Myklebust, R. Ree and T. Arnesen, The world of protein acetylation, *Biochim. Biophys. Acta (BBA) – Biophys. Incl. Photosynth.*, 2016, **1864**(10), 1372–1401.
52 J. R. Mekala, P. Ramalingam, N. R. Moparthi, and V. K. Kutala, ROS Modulatory Role of HDAC Inhibitors in Cancer Cells, In. *Handbook of Oxidative Stress in Cancer: Therapeutic Aspects*, Springer Singapore, Singapore, 2022, p. 1–28.
53 R. Zhang, M. J. Piao, K. C. Kim, A. D. Kim, J. Y. Choi, J. Choi, *et al.*, Endoplasmic reticulum stress signaling is involved in silver nanoparticles-induced apoptosis, *Int. J. Biochem. Cell Biol.*, 2012, **44**(1), 224–232.
54 J. C. Simard, I. Durocher and D. Girard, Silver nanoparticles induce irremediable endoplasmic reticulum stress leading to unfolded protein response dependent apoptosis in breast cancer cells, *Apoptosis*, 2016, **21**(11), 1279–1290.
55 M. Śniegocka, F. Liccardo, F. Fazi and S. Masciarelli, Understanding ER homeostasis and the UPR to enhance treatment efficacy of acute myeloid leukemia, *Drug Resist. Updates*, 2022, **64**, 100853.
56 A. H. Schönthal, Endoplasmic Reticulum Stress: Its Role in Disease and Novel Prospects for Therapy, *Cientifica*, 2012, **2012**, 1–26.
57 S. S. Cao and R. J. Kaufman, Endoplasmic Reticulum Stress and Oxidative Stress in Cell Fate Decision and Human Disease, *Antioxid. Redox Signaling*, 2014, **21**(3), 396–413.
58 I. R. Indran, G. Tufo, S. Pervaiz and C. Brenner, Recent advances in apoptosis, mitochondria and drug resistance in cancer cells, *Biochim. Biophys. Acta Bioenerg.*, 2011, **1807**(6), 735–745.
59 S. Zhang, S. Rao, M. Yang, C. Ma, F. Hong and S. Yang, Role of Mitochondrial Pathways in Cell Apoptosis during He-Patic Ischemia/Reperfusion Injury, *Int. J. Mol. Sci.*, 2022, **23**(4), 2357.
60 S. Chen, Q. Li, H. Shi, F. Li, Y. Duan and Q. Guo, New insights into the role of mitochondrial dynamics in oxidative stress-induced diseases, *Biomed. Pharmacother.*, 2024, **178**, 117084.
61 R. Scully, A. Panday, R. Elango and N. A. Willis, DNA double-strand break repair-pathway choice in somatic mammalian cells, *Nat. Rev. Mol. Cell Biol.*, 2019, **20**(11), 698–714.
62 E. A. Slee, M. T. Harte, R. M. Kluck, B. B. Wolf, C. A. Casiano, D. D. Newmeyer, *et al.*, Ordering the Cytochrome c–initiated Caspase Cascade: Hierarchical Activation of Caspases-2, -3, -6, -7, -8, and -10 in a Caspase-9–dependent Manner, *J. Cell Biol.*, 1999, **144**(2), 281–292.
63 E. A. Slee, C. Adrain and S. J. Martin, Executioner Caspase-3, -6, and -7 Perform Distinct, Non-redundant Roles during the Demolition Phase of Apoptosis, *J. Biol. Chem.*, 2001, **276**(10), 7320–7326.
64 G. Sahoo, D. Samal, P. Khandayataray and M. K. Murthy, A Review on Caspases: Key Regulators of Biological Activities and Apoptosis, *Mol. Neurobiol.*, 2023, **60**(10), 5805–5837.